The scattering of light from two-dimensional randomly rough surfaces

T.A. Leskova[a], P.A. Letnes[b], A.A. Maradudin[a], T. Nordam[b] and I. Simonsen[b]

[a]Department of Physics and Astronomy and Institute for Surface and Interface Science
University of California, Irvine CA 92697, U.S.A.
[b]Department of Physics, Norwegian University of Science and Technology (NTNU)
NO-7491 Trondheim, Norway

ABSTRACT

We present results, obtained by rigorous computational approaches, for light of p- and s-polarization scattered from two-dimensional, randomly rough, perfectly conducting, lossy metallic, and dielectric surfaces. The perfectly conducting surfaces we study are characterized by an isotropic power spectrum of the surface roughness and by an anisotropic power spectrum. The mean differential reflection coefficient and the full angular distribution of the intensity of the scattered light are calculated for the perfectly conducting and metal surfaces. From the latter calculations it is found that the computational approach used in these calculations conserves energy in the scattering from a perfectly conducting and from a lossless metal surface with an error that is smaller than 0.5%. Finally, we presents results obtained by a numerical, nonperturbative, solution of the reduced Rayleigh equation for the scattering of p- and s-polarized light from two-dimensional randomly rough, metallic and dielectric surfaces. We show that the results for the metallic surface are in good agreement with results for the same metallic surface obtained by the rigorous computational approach.

Keywords: randomly rough surfaces; mean differential reflection coefficient; impedance boundary condition; reduced Rayleigh equation; Müller integral equations; Franz formulas; Stratton–Chu equation; scattering

1. INTRODUCTION

Despite the significant advances that have been made in the last 15 years or so in approaches to the calculation of the scattering of light from two-dimensional randomly rough perfectly conducting[1–8] and penetrable[6,9–14] surfaces, such calculations remain computationally intensive, and need further improvements in the methods used in carrying them out. In this paper we review some of our recent work devoted to this problem, and present some new results. The emphasis will be on the results obtained and their significance, but the methods by which the results were obtained will be sketched out.

The physical system we consider in this paper consists of vacuum in the region $x_3 > \zeta(\mathbf{x}_\parallel)$, where $\mathbf{x}_\parallel = (x_1, x_2, 0)$, and the scattering medium in the region $x_3 < \zeta(\mathbf{x}_\parallel)$ (Fig. 1). The latter will be a perfect conductor, a metal, or a dielectric. The surface profile function $\zeta(\mathbf{x}_\parallel)$ is assumed to be a single-valued function of $\mathbf{x}_\parallel$ that is at least twice differentiable with respect to x_1 and x_2, and constitutes a stationary, zero-mean, Gaussian random process defined by $\left\langle \zeta(\mathbf{x}_\parallel)\zeta(\mathbf{x}'_\parallel)\right\rangle = \delta^2 W(\mathbf{x}_\parallel - \mathbf{x}'_\parallel)$. The angle brackets here denote an average over the ensemble of realizations of the surface profile function, and $\delta = \left\langle \zeta^2(\mathbf{x}_\parallel)\right\rangle^{\frac{1}{2}}$ is the rms height of the surface. The power spectrum of the surface roughness is defined by

$$g(\mathbf{k}_\parallel) = \int \mathrm{d}^2 x_\parallel \, W(\mathbf{x}_\parallel) \exp\left(-\mathrm{i}\mathbf{k}_\parallel \cdot \mathbf{x}_\parallel\right), \tag{1}$$

where $\mathbf{k}_\parallel = (k_1, k_2, 0)$. Each realization of the surface profile function is generated numerically by a two-dimensional version of the filtering method used in [15], which is based on the power spectrum (1).

This paper is organized as follows. Scattering from two-dimensional randomly rough perfectly conducting surfaces will be discussed in Section 2, both when the surface roughness is characterized by an an isotropic power spectrum and when it is characterized by an anisotropic power spectrum. In Section 3 scattering from a

Optical Complex Systems: OCS11, edited by Gérard Berginc, Proc. of SPIE Vol. 8172
817209 · © 2011 SPIE · CCC code: 0277-786X/11/$18 · doi: 10.1117/12.899304

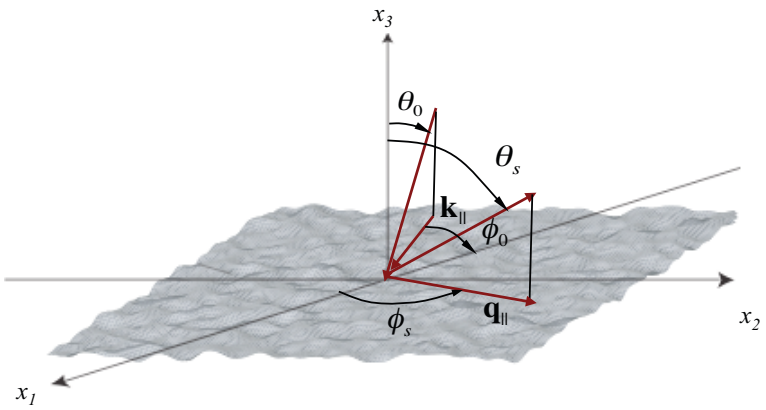

Figure 1. A sketch of the studied scattering geometry. The figure also shows the coordinate system used, angles of incidence (θ_0, ϕ_0) and scattering (θ_s, ϕ_s), and the corresponding transverse wavevectors $\mathbf{k}_\parallel$ and $\mathbf{q}_\parallel$, respectively.

two-dimensional randomly rough penetrable surface is considered, specifically scattering from a metallic surface and from a dielectric surface. Section 4 is devoted to a presentation of results obtained from a purely numerical, nonperturbative, solution of the reduced Rayleigh equation for the scattering of polarized light from a two-dimensional, randomly rough, penetrable surface. A discussion of the results obtained, and conclusions drawn from them, in Section 5, concludes this paper.

2. A PERFECTLY CONDUCTING SURFACE

2.1 Mathematical Formulation

The starting point for the calculation of the electromagnetic field scattered from a two-dimensional rough perfectly conducting surface is the Stratton–Chu formula[16] for the magnetic field in the vacuum

$$\theta(x_3 - \zeta(\mathbf{x}_\parallel))\,\mathbf{H}^{>}(\mathbf{x}|\omega) = \mathbf{H}(\mathbf{x}|\omega)_{\rm inc} + \frac{1}{4\pi}\int \mathrm{d}^2 x'_\parallel \;\; [\boldsymbol{\nabla} g_0(\mathbf{x}|\mathbf{x}')]|_{x'_3=\zeta(\mathbf{x}'_\parallel)} \times \mathbf{J}_H(\mathbf{x}'_\parallel|\omega), \tag{2}$$

where $\theta(z)$ is the Heaviside unit step function, and $\mathbf{H}(\mathbf{x}|\omega)_{\rm inc}$ is the magnetic component of the incident field. In writing Eq. (2) we have assumed the time dependence $\exp(-\mathrm{i}\omega t)$ for the field, but have not indicated this explicitly.

The function $g_0(\mathbf{x}|\mathbf{x}')$ is the scalar free-space Green's function,

$$g_0(\mathbf{x}|\mathbf{x}') = \frac{\exp\left[\mathrm{i}\frac{\omega}{c}\,|\mathbf{x}-\mathbf{x}'|\right]}{|\mathbf{x}-\mathbf{x}'|} \tag{3a}$$

$$= \int \frac{\mathrm{d}^2 q_\parallel}{(2\pi)^2}\,\frac{2\pi\mathrm{i}}{\alpha_0(q_\parallel)} \exp\left[\mathrm{i}\mathbf{q}_\parallel\cdot(\mathbf{x}_\parallel - \mathbf{x}'_\parallel)\right] \exp\left[\mathrm{i}\alpha_0(q_\parallel)|x_3 - x'_3|\right], \tag{3b}$$

where ω and c are the angular frequency and speed of light in vacuum, respectively, while $\alpha_0(q_\parallel) = [(\omega/c)^2 - q_\parallel^2]^{\frac{1}{2}}$, with $\mathrm{Re}\,\alpha_0(q_\parallel) > 0$, $\mathrm{Im}\,\alpha_0(q_\parallel) > 0$. The electric surface current $\mathbf{J}_H(\mathbf{x}_\parallel|\omega)$ is defined by $\mathbf{J}_H(\mathbf{x}_\parallel|\omega) = [\mathbf{n} \times \mathbf{H}^{>}(\mathbf{x}|\omega)]_{x_3=\zeta(\mathbf{x}_\parallel)}$, where $\mathbf{n} = (-\zeta_1(\mathbf{x}_\parallel), -\zeta_2(\mathbf{x}_\parallel), 1)$ and $\zeta_j(\mathbf{x}_\parallel) \equiv \partial\zeta(\mathbf{x}_\parallel)/\partial x_j$ $(j = 1, 2)$. On evaluating Eq. (2) at $x_3 = \zeta(\mathbf{x}_\parallel) + \eta$ and at $x_3 = \zeta(\mathbf{x}_\parallel) - \eta$, where η is a positive infinitesimal, adding the resulting two equations, and taking the vector cross product of the sum with $\mathbf{n}$, we obtain the integral equation satisfied by $\mathbf{J}_H(\mathbf{x}_\parallel|\omega)$,

$$\mathbf{J}_H(\mathbf{x}_\parallel|\omega) = 2\mathbf{J}_H^{(i)}(\mathbf{x}_\parallel|\omega) + \frac{1}{2\pi} P\int \mathrm{d}^2 x'_\parallel\; \mathbf{n} \times \left\{ [\![\boldsymbol{\nabla} g_0(\mathbf{x}|\mathbf{x}')]\!] \times \mathbf{J}_H(\mathbf{x}'_\parallel|\omega)\right\}, \tag{4}$$

where $\mathbf{J}_H^{(i)}(\mathbf{x}_\parallel|\omega)_{\rm inc} = \mathbf{n}\times\mathbf{H}(\mathbf{x}|\omega)_{\rm inc}|_{x_3=\zeta(\mathbf{x}_\parallel)}$, P denotes the Cauchy principal value, and we have introduced the definition

$$[\![f(\mathbf{x}|\mathbf{x}')]\!] \;=\; f(\mathbf{x}|\mathbf{x}')\Big|_{\substack{x_3=\zeta(\mathbf{x}_\parallel)\\ x_3'=\zeta(\mathbf{x}_\parallel')}}. \tag{5}$$

Because $\mathbf{n}\cdot\mathbf{J}_H(\mathbf{x}_\parallel|\omega)=0$, only two components of $\mathbf{J}_H(\mathbf{x}_\parallel|\omega)$ are independent. We choose them to be $J_H(\mathbf{x}_\parallel|\omega)_1$ and $J_H(\mathbf{x}_\parallel|\omega)_2$, and obtain $J_H(\mathbf{x}_\parallel|\omega)_3$ from

$$J_H(\mathbf{x}_\parallel|\omega)_3 = \zeta_1(\mathbf{x}_\parallel)J_H(\mathbf{x}_\parallel|\omega)_1 + \zeta_2(\mathbf{x}_\parallel)J_H(\mathbf{x}_\parallel|\omega)_2. \tag{6}$$

The two coupled, inhomogeneous, two-dimensional integral equations satisfied by $J_H(\mathbf{x}_\parallel|\omega)_{1,2}$ are solved by converting them into matrix equations. This is done by generating a realization of the surface profile function on a grid of N^2 points within a square region of the x_1x_2 plane of edge L, where the discretization intervals for both directions are $\Delta x = L/N$. The integrals over this region are carried out by means of a two-dimensional version of the extended midpoint method,[17] and the values of $J_H(\mathbf{x}_\parallel|\omega)_1$ and $J_H(\mathbf{x}_\parallel|\omega)_2$ are calculated at the points of this grid. The resulting matrix equations are solved by means of the biconjugate gradient stabilized method.[18] The values of $J_H(\mathbf{x}_\parallel|\omega)_3$ are then obtained by the use of Eq. (6).

In these calculations the incident electric field has the form of a p- or s-polarized Gaussian beam, propagating in the direction of $\mathbf{k} = (\omega/c)(\sin\theta_0\cos\phi_0, \sin\theta_0\sin\phi_0, -\cos\theta_0)$. In the case that $\mathbf{k}_\parallel = k_\parallel\hat{\mathbf{x}}_1$, it is given by

$$\mathbf{E}_\nu(\mathbf{x}|\omega)_{\rm inc} \;=\; \int\limits_{q_\parallel<\frac{\omega}{c}} {\rm d}^2q_\parallel\; \hat{\boldsymbol{\mathcal{E}}}_\nu^{(i)}(\mathbf{q}_-|\omega)\exp\left[{\rm i}\mathbf{q}_-\cdot\mathbf{x}\right]\; W(\mathbf{q}_\parallel|\mathbf{k}_\parallel), \tag{7}$$

where $\nu = p$ or s, $\mathbf{q}_\pm(\mathbf{q}_\parallel,\omega) = \mathbf{q}_\parallel \pm \alpha_0(q_\parallel)\hat{\mathbf{x}}_3$, and $W(\mathbf{q}_\parallel|\mathbf{k}_\parallel)$ is

$$W(\mathbf{q}_\parallel|\mathbf{k}_\parallel) = \frac{w^2}{2\pi}\exp\left[-\frac{w^2}{2}(\mathbf{q}_\parallel-\mathbf{k}_\parallel)^2\right]. \tag{8}$$

For an incident field that is p polarized

$$\hat{\boldsymbol{\mathcal{E}}}_p^{(i)}(\mathbf{q}_-|\omega) \;=\; \frac{\alpha_0(q_\parallel)\hat{\mathbf{x}}_1 + q_1\hat{\mathbf{x}}_3}{[q_1^2+\alpha_0^2(q_\parallel)]^{\frac{1}{2}}}, \tag{9a}$$

while for an incident field that is s polarized

$$\hat{\boldsymbol{\mathcal{E}}}_s^{(i)}(\mathbf{q}_-|\omega) \;=\; \frac{q_1q_2\hat{\mathbf{x}}_1 - [q_1^2+\alpha_0^2(q_\parallel)]\hat{\mathbf{x}}_2 - q_2\alpha_0(q_\parallel)\hat{\mathbf{x}}_3}{\frac{\omega}{c}[q_1^2+\alpha_0^2(q_\parallel)]^{\frac{1}{2}}}. \tag{9b}$$

The scattered electric field, written in terms of $\mathbf{J}_H(\mathbf{x}_\parallel|\omega)$, is

$$\mathbf{E}(\mathbf{x}|\omega)_{\rm sc} \;=\; \int\frac{{\rm d}^2q_\parallel}{(2\pi)^2}\;\left[\mathcal{E}_p(\mathbf{q}_+|\omega)\hat{\boldsymbol{\gamma}}_p(\mathbf{q}_+|\omega) + \mathcal{E}_s(\mathbf{q}_+|\omega)\hat{\boldsymbol{\gamma}}_s(\mathbf{q}_+|\omega)\right]\exp\left[{\rm i}\mathbf{q}_+\cdot\mathbf{x}\right], \tag{10}$$

where

$$\hat{\boldsymbol{\gamma}}_p(\mathbf{q}_+|\omega) \;=\; \frac{-\alpha_0(q_\parallel)\hat{\mathbf{q}}_\parallel + q_\parallel\hat{\mathbf{x}}_3}{\omega/c} \tag{11a}$$

$$\hat{\boldsymbol{\gamma}}_s(\mathbf{q}_+|\omega) \;=\; \hat{\mathbf{q}}_\parallel\times\hat{\mathbf{x}}_3, \tag{11b}$$

and $(\nu = p, s)$

$$\mathcal{E}_\nu(\mathbf{q}_+|\omega) \;=\; -\frac{(\omega/c)}{2\alpha_0(q_\parallel)}\int{\rm d}^2x_\parallel\;\hat{\boldsymbol{\gamma}}_\nu(\mathbf{q}_+|\omega)\cdot\mathbf{J}_H(\mathbf{x}_\parallel|\omega)\exp\left[-{\rm i}\mathbf{q}_\parallel\cdot\mathbf{x}_\parallel - {\rm i}\alpha_0(q_\parallel)\zeta(\mathbf{x}_\parallel)\right]. \tag{12}$$

The differential reflection coefficient $(\partial R/\partial\Omega_s)$ is defined such that $(\partial R/\partial\Omega_s)\mathrm{d}\Omega_s$ is the fraction of the total time-averaged flux incident on the surface that is scattered into the element of solid angle $\mathrm{d}\Omega_s$ about the scattering direction (θ_s, ϕ_s). Since we are studying the scattering of light from a randomly rough surface, it is the average of this quantity over the ensemble of realizations of the surface profile function that we need to calculate. The mean differential reflection coefficient for the scattering of light of polarization β, the projection of whose wave vector on the mean scattering surface is $\mathbf{k}_\parallel$, into light of polarization α, the projection of whose wave vector on the mean scattering surface is $\mathbf{q}_\parallel$, is given by

$$\left\langle \frac{\partial R_{\alpha\beta}}{\partial\Omega_s} \right\rangle = \frac{1}{4\pi^2}\left(\frac{\omega}{c}\right)^3 \cos^2\theta_s \frac{\left\langle |\mathcal{E}_\alpha(\mathbf{q}_+|\omega)|^2 \right\rangle}{p_{\mathrm{inc}}}, \tag{13}$$

where for both polarizations of the incident light,

$$p_{\mathrm{inc}} = w^4 \int\limits_{q_\parallel < \frac{\omega}{c}} \mathrm{d}^2 q_\parallel \; \alpha_0(q_\parallel) \exp\left[-w^2(\mathbf{q}_\parallel - \mathbf{k}_\parallel)^2\right]. \tag{14}$$

The dependence of the right-hand side of this equation on the polarization index β is through the dependence of the amplitude $\mathcal{E}_\alpha(\mathbf{q}_+|\omega)$ on the surface current $\mathbf{J}_H(\mathbf{x}_\parallel|\omega)$ in Eq. (12). The surface current satisfies Eq. (4) in which the inhomogeneous term depends on the incident field and hence on its polarization $\beta = p, s$. Therefore $\mathcal{E}_\alpha(\mathbf{q}_+|\omega)$ depends implicitly on the polarization β of the incident field and consequently so does the mean differential reflection coefficient.

If one is interested in nonspecular effects, it is the contribution to the mean differential reflection coefficient from the light that has been scattered incoherently (diffusely) that is of interest. It is given by

$$\left\langle \frac{\partial R_{\alpha\beta}}{\partial\Omega_s} \right\rangle_{\mathrm{incoh}} = \frac{1}{4\pi^2}\left(\frac{\omega}{c}\right)^3 \cos^2\theta_s \frac{\left\langle \left|\mathcal{E}_\alpha(\mathbf{q}_+|\omega)\right|^2 \right\rangle - \left|\left\langle \mathcal{E}_\alpha(\mathbf{q}_+|\omega)\right\rangle\right|^2}{p_{\mathrm{inc}}}. \tag{15}$$

We now turn to some results obtained on the basis of this method.

2.2 Results for a Perfectly Conducting Surface

2.2.1 An Isotropic Roughness Power Spectrum

The first set of calculations were carried out for a two-dimensional randomly rough perfectly conducting surface defined by an isotropic surface height autocorrelation function, *i.e.* one that depends on the vector $\mathbf{x}_\parallel$ only through its magnitude. We have chosen for it the Gaussian form $W(\mathbf{x}_\parallel) = \exp(-x_\parallel^2/a^2)$. The characteristic length a is called the transverse correlation length of the surface roughness. The power spectrum of the surface, given by Eq. (1), in this case has the form

$$g(\mathbf{k}_\parallel) = \pi a^2 \exp\left(-\frac{k_\parallel^2 a^2}{4}\right). \tag{16}$$

We have carried out calculations of the scattering of p-polarized light from such a surface with an rms height $\delta = \lambda$ and a transverse correlation length $a = 2\lambda$, where λ is the wavelength of the incident field in vacuum. The incident field had the form of a Gaussian beam, Eq. (7), with $w = 4\lambda$. The surface, covering an area $L^2 = 16\lambda \times 16\lambda$ in the mean surface plane, was generated at the points of a 112×112 grid of mesh size $\Delta x = \lambda/7$ for both directions.

In Fig. 2 we plot the mean differential reflection coefficients as functions of the polar scattering angle θ_s for the in-plane $(\phi_s = 0°, 180°)$ and out-of-plane $(\phi_s = \pm 90°)$ co-$(p \to p)$ and cross-$(p \to s)$ polarized scattering when a p-polarized Gaussian beam is incident on the surface at angles of incidence (θ_0, ϕ_0) given by $(0°, 0°)$ and $(20°, 0°)$. Results obtained for 12 000 realizations of the surface profile function were averaged to obtain these figures. The calculations for each realization of the surface profile function required 76 CPU seconds on an Intel Core 2 CPU (Q9550) operating at 2.83 GHz and running the Linux operating system. For the roughness

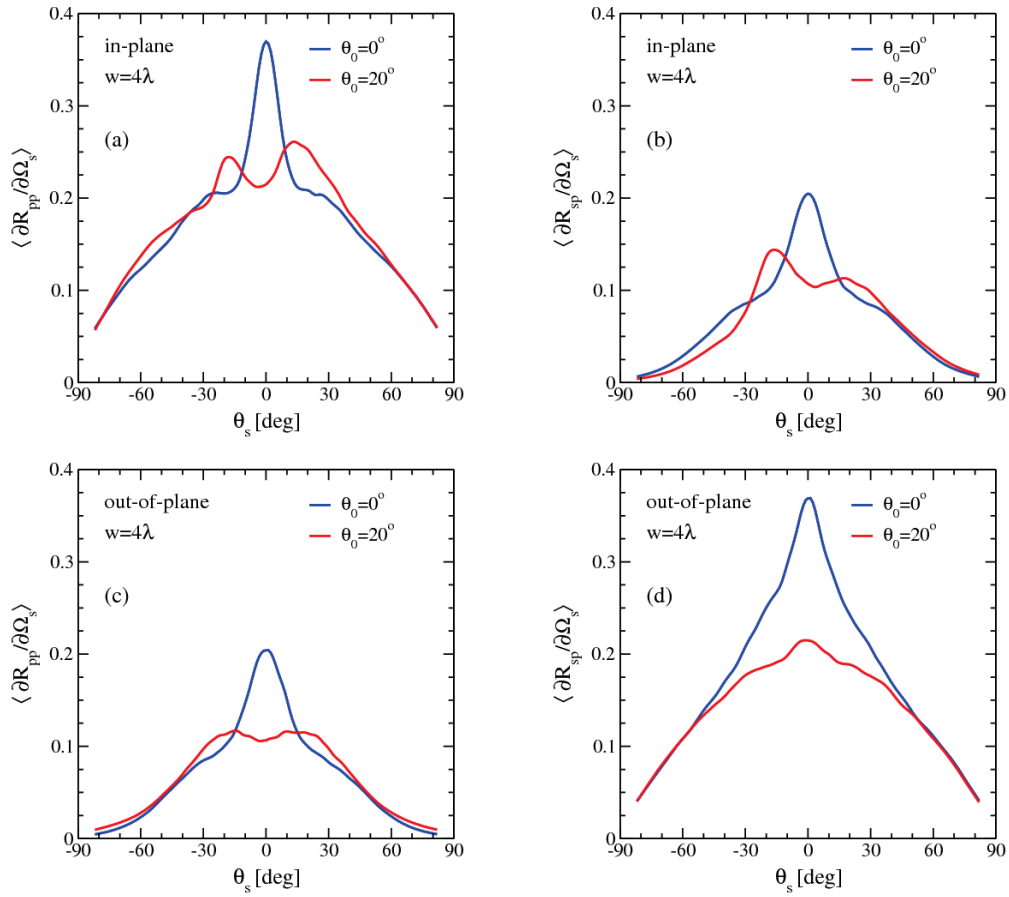

Figure 2. The mean differential reflection coefficients, $\langle \partial R_{\alpha\beta}/\partial\Omega_s \rangle$ ($\beta \to \alpha$), as functions of the polar scattering angle θ_s for the in-plane ($\phi_s = \phi_0$ or $\phi_s = \phi_0 + 180^\circ$) (a) co-polarized ($p \to p$) and (b) cross-polarized scattering ($p \to s$), and the out-of-plane ($\phi_s = \phi_0 \pm 90^\circ$) (c) co-polarized ($p \to p$) and (d) cross-polarized scattering ($p \to s$) of a p-polarized incident beam ($\beta = p$) of width $w = 4\lambda$ ($\theta_0 = 0^\circ$ and $\theta_0 = 20^\circ$; $\phi_0 = 0^\circ$) scattered from a Gaussian randomly rough perfectly conducting surface. The Gaussian correlated surface had a correlation length $a = 2\lambda$ and an rms height $\delta = \lambda$. To facilitate comparison between the various configurations presented in this figure, notice that we have used similar scales for all ordinate axes. Moreover, to simplify the presentation of the figures, a convention was adopted where negative (positive) values of θ_s correspond to $\phi_s = \phi_0 + 180^\circ$ ($\phi_s = \phi_0$). (After Ref. 7).

parameters assumed in these calculations the contribution to the mean differential reflection coefficient from the light scattered coherently is smaller than the contribution from the light scattered incoherently by a factor of approximately 10^{-4}.

There is no single scattering contribution to the mean differential reflection coefficient in the cases of in-plane cross-polarized [Fig. 2(b)] and out-of-plane co-polarized [Fig. 2(c)] scattering.[1] What is plotted in these figures therefore is due to multiple scattering only. The results plotted in Figs. 2(a) and 2(d) contain a contribution from single-scattering processes.

The peaks in the retroreflection directions in the results for in-plane co-polarized scattering [Fig. 2(a)] are enhanced backscattering peaks.[19–22] However, as we will see from the full angular distribution of the intensity of the scattered light, the structures seen as peaks in the results for in-plane cross-polarized scattering [Fig. 2(b)] are not real peaks. The results that the out-of-plane co- and cross-polarized scattering [Figs. 2(c) and 2(d)] are even functions of θ_s are consequences of the scattering geometry, namely that $\phi_0 = 0^\circ$, $\phi_s = \pm 90^\circ$, and the isotropy of the power spectrum of the surface roughness.

The full angular distribution of the intensity of the scattered light is presented as contour plots in Fig. 3,

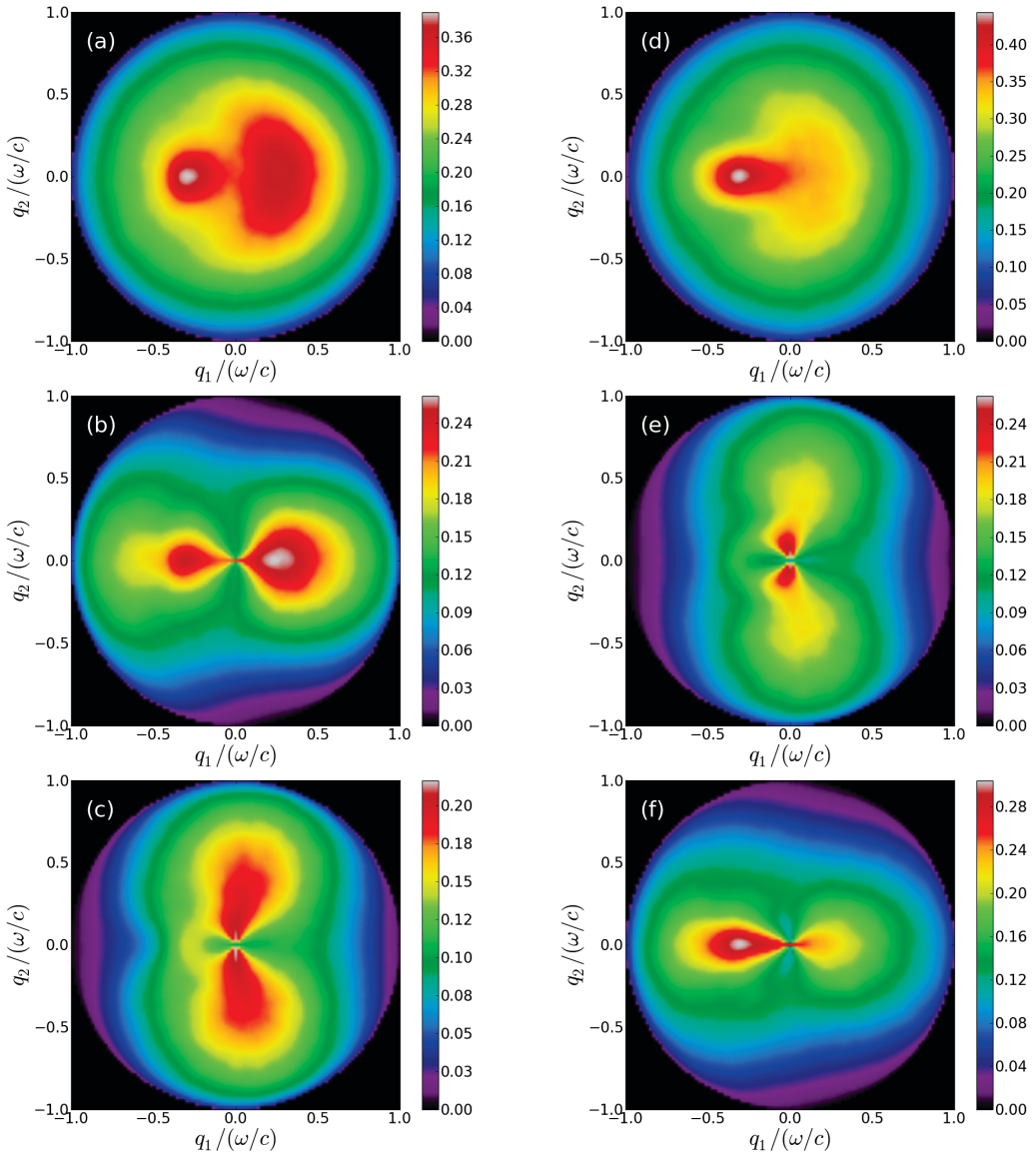

Figure 3. The complete angular distributions of the mean differential reflection coefficient, $\langle \partial R_{\alpha\beta}/\partial\Omega_s \rangle$, for the scattering of an β-polarized Gaussian beam incident on the surface at polar angle $\theta_0 = 20^\circ$ and azimuthal angle $\phi_0 = 0^\circ$. The perfectly conducting rough surface was characterized by a Gaussian height distribution of rms-value $\delta = \lambda$ and a Gaussian correlation function of transverse correlation length $a = 2\lambda$. The incident beam was p polarized in Figs. 3(a)–(c) [left column], and s polarized in Figs. 3(d)–(f) [right column]. Moreover, in the top two figures [Figs. 3(a) and (d)] the polarization of the scattered light was not recorded; in Figs. 3(b) and (e) [central row] only p-polarized scattered light was recorded; while the bottom two figures correspond to recording only s-polarized scattered light [Figs. 3(c) and (f)]. The rough surface, covering an area $16\lambda \times 16\lambda$, was discretized at a grid of 112×112 points corresponding to a discretization interval $\lambda/7$ for both directions. The presented figures were obtained by averaging results for the differential reflection coefficient obtained for 12 000 surface realizations. (After Ref. 7).

which correspond to polar and azimuthal angles of incidence $(\theta_0, \phi_s) = (20^\circ, 0^\circ)$, when the incident beam is p polarized and the scattered light is p and s polarized. In Fig. 3(a) we present a contour plot of the mean differential reflection coefficient for the scattering of p-polarized light into both p- and s-polarized scattered light, *i.e.* the polarization state of the scattered light was not recorded. It is seen that there is a pronounced enhanced backscattering peak in the retroreflection direction at $\theta_s = 20^\circ$ and $\phi_s = 180^\circ$. From Figs. 3(b) and 3(c),

where only p-polarized light or s-polarized scattered light is recorded, respectively, we see that the co-polarized scattering displays a structure that is elongated along the plane of incidence, while the cross-polarized scattering has a scattering pattern that is elongated perpendicular to this plane. In principle an enhanced backscattering peak should be present in the retroreflection direction in both co- and cross-polarized scattering.[20–22] However, for the roughness parameters assumed in this work, instead of a well-defined peak in the retroreflection direction we see a ridge of constant enhanced intensity in parts of the region $q_1 < 0$, forming a semicircle of constant polar scattering angle $\theta_s \approx \theta_0 = 20°$, with $90° < \phi_s < 270°$ [Fig. 3(c)]. In precisely the retroreflection direction, $\theta_s = 20°$ and $\phi_s = 180°$, there is little, if any, additional enhancement in the cross-polarized scattering compared to the intensities at other values of ϕ_s in the interval $[90°, 270°]$. We speculate that the enhancement ridge seen in Fig. 3(c) is a constructive interference effect similar to the effect underlying enhanced backscattering.

We note that if we had examined only the in-plane and out-of-plane results for the same angle of incidence, the peak observed in Fig. 2(b) for $\theta_0 = 20°$ could easily have been interpreted as the well-localized feature in the retroreflection direction similar to the one present for co-polarized scattering in Fig. 3(b). Thus the angular distributions of the intensities of the scattered light, such as those presented in Fig. 3, can provide information that helps in better understanding multiple scattering phenomena.

When the incident beam was s polarized, we obtain the results presented in Figs. 3(d)–(f). Also here an enhanced backscattering peak is observed, and the intensity distributions of the co- and cross-polarized scattered light are oriented along and perpendicular to the plane of incidence, respectively.

A necessary, but not sufficient, criterion for the accuracy of a scattering calculation is that energy be conserved in the scattering process. In scattering from a perfectly conducting surface this requires that the total time-averaged scattered flux must equal the total time-averaged incident flux. This requirement can be stated as

$$U_\beta(\theta_0, \phi_0) = \sum_{\alpha=p,s} \int \mathrm{d}\Omega_s \left\langle \frac{\partial R_{\alpha\beta}}{\partial \Omega_s} \right\rangle = 1 \qquad \beta = p, s. \tag{17}$$

Under the conditions assumed in obtaining the results presented in Figs. 2 and 3, the value of $U_p(\theta_0, \phi_0)$ and $U_s(\theta_0, \phi_0)$ were calculated to be 0.9962 and 0.9966, respectively. Consequently, the computational approach outlined in Section 2 conserves energy in the scattering process with an error that is smaller than 0.5%. This error is expected to be reduced further by decreasing the sampling interval Δx and/or by increasing the area (L^2) of the the mean surface.

2.2.2 An Anisotropic Roughness Power Spectrum

The existing computational studies of the scattering of light from two-dimension randomly rough perfectly conducting surfaces[1–7] have been based on the assumption that the surface profile function $\zeta(\mathbf{x}_\parallel)$ is a stationary, zero-mean, *isotropic*, Gaussian random process. Very little work has been devoted to the case where $\zeta(\mathbf{x}_\parallel)$ is an *anisotropic* random process. In this section we present results obtained by the rigorous computational approach described in Section 2.1 for the light scattered from a two-dimensional, randomly rough, perfectly conducting surface defined by a surface profile function that is a stationary, zero-mean, anisotropic, Gaussian random process.

The surface we assume in these calculations is defined by a surface height autocorrelation function that has an anisotropic Gaussian form, $W(\mathbf{x}_\parallel) = \exp[-(x_1/a_1)^2 - (x_2/a_2)^2]$ where, for specificity, we assume that $a_1 < a_2$. Thus, we will refer to the x_1 and x_2 axes as the minor and major axes of the anisotropy, respectively. The power spectrum of the surface roughness, defined by Eq. (1), in the present case has the form

$$g(\mathbf{k}_\parallel) \quad = \quad \pi a_1 a_2 \exp\left[-\frac{k_1^2 a_1^2}{4} - \frac{k_2^2 a_2^2}{4}\right], \tag{18}$$

and is elongated along the minor anisotropy axis.

To provide a reference against which results for the angular distribution of the fields scattered from an anisotropic random surface can be compared, we first present, in Fig. 4, contour plots of the angular distributions of the fields scattered from an *isotropic* random surface. The incident field is a p-polarized beam with the width

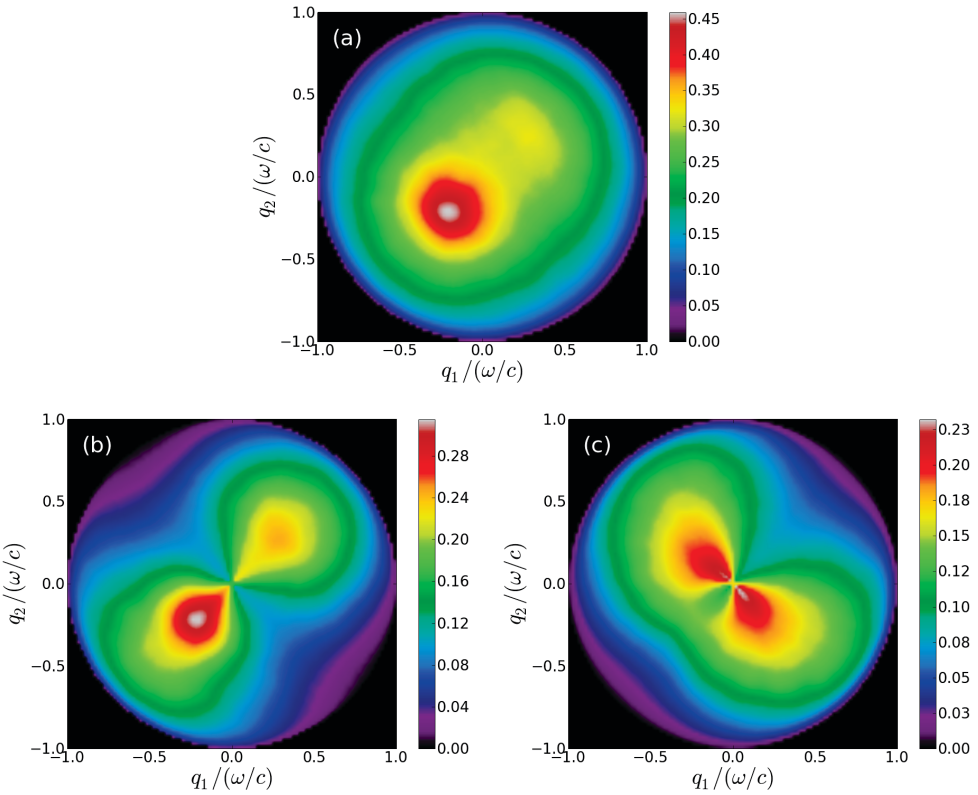

Figure 4. A p-polarized beam of wavelength λ and width $w = 4\lambda$ is scattered from an *isotropic* perfectly conducing rough surface characterized by a Gaussian height distribution of rms-value $\delta = \lambda/2$ and a Gaussian correlation function of correlation lengths $a_1 = a_2 = \lambda$. The panels show contour plots of the full angular distributions of the mean differential reflection coefficient, $\langle \partial R_{\alpha p}/\partial \Omega_s \rangle$, obtained by a rigorous computer simulation approach for the scattering of the beam incident on the rough surface at a polar angle $\theta_0 = 20^\circ$ and an azimuthal angle $\phi_0 = 45^\circ$. The three panels correspond to various configurations for the polarization of the scattered light. They are: (a) the polarization of the scattered light is not recorded [$\alpha = p, s$]; (b) only p-polarized scattered light is measured [$\alpha = p$]; and (c) only s-polarized scattered light is recorded [$\alpha = s$]. The rough surface, covering an area $16\lambda \times 16\lambda$, was discretized on a grid of 112×112 points corresponding to a discretization interval $\lambda/7$ for both directions. The presented figures were obtained by averaging results for the differential reflection coefficient obtained for 6 000 surface realizations. (After Ref. 8).

parameter $w = 4\lambda$, where λ is the wavelength of the field. The polar and azimuthal angles of incidence are $(\theta_0, \phi_0) = (20^\circ, 45^\circ)$. The surface is characterized by the Gaussian power spectrum (16), with a correlation length $a = \lambda$. The rms height of the surface is $\delta = \lambda/2$. The surface was generated on the same grid as the surface studied in Section 2.2.1. The mean differential reflection coefficient was obtained as the arithmetic average of results obtained for 6000 realizations of the surface profile function. The three panels in this figure correspond to different choices for the polarization of the scattered light. Thus, in obtaining Fig. 4(a) the polarization of the scattered light was not recorded; in obtaining Fig. 4(b) only the p-polarized component of the scattered light was recorded; while in obtaining Fig. 4(c) only the s-polarized component of the scattered light was recorded.

We see from these results that the co-polarized ($p \to p$) scattering has a dipole-like angular distribution with the main intensity oriented parallel to the plane of incidence [Fig. 4(b)]. In contrast the cross-polarized ($p \to s$) scattering has its main intensity distribution oriented perpendicular to the plane of incidence [Fig. 4(c)]. In both cases the intensity distributions are symmetric with respect to the plane of incidence, and the scattered intensity patterns simply rotate as the azimuthal angle of incidence ϕ_0 is changed. When the polarization of the scattered light is not recorded [Fig. 4(a)], the pronounced peak in the retroreflection direction ($\theta_s = \theta_0, \phi_s = \phi_0 + 180^\circ$) is the enhanced backscattering peak.

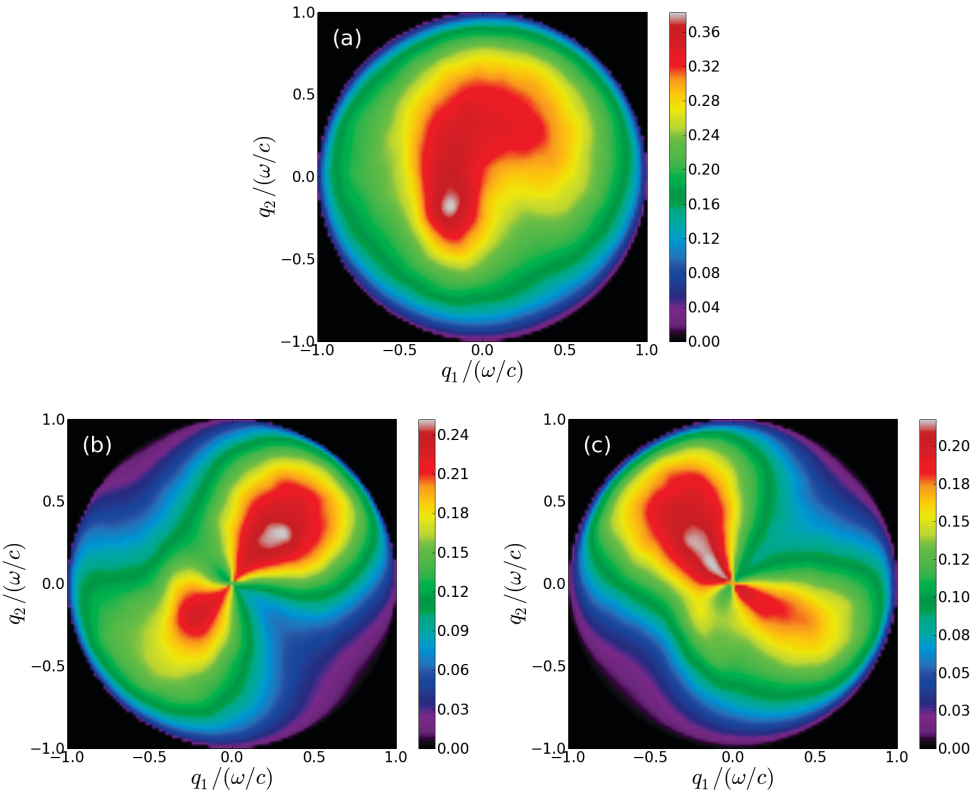

Figure 5. Same as Fig. 4 with the only difference that now the rough surface is *weakly anisotropic* and characterized by the correlation lengths $a_1 = \lambda$ and $a_2 = 1.5\lambda$. (After Ref. 8).

Turning now to the scattering from an anisotropic surface, in Fig. 5 we present contour plots of the full angular distributions of the mean differential reflection coefficients when the randomly rough surface is defined by the power spectrum (18) with $a_1 = \lambda$ and $a_2 = 1.5\lambda$. The remaining experimental and computational parameters have the values used in obtaining the results presented in Fig. 4. The three panels correspond to different choices for the polarization of the scattered light. In obtaining Fig. 5(a) the polarization of the scattered light was not recorded; in obtaining Fig. 5(b) only the p-polarized component of the scattered light was recorded; while in obtaining Fig. 5(c) only the s-polarized component of the scattered light was recorded. Unlike in the scattering of light from an isotropic surface, the intensity distribution of light scattered from an anisotropic surface in general is not symmetric with respect to the plane of incidence. It is only when the plane of incidence is parallel to either the minor or the major axis of the anisotropy that this type of symmetry obtains.

The dipole-like angular intensity patterns in Figs. 5(b) and 5(c) are no longer symmetric with respect to the plane of incidence, as their isotropic equivalents are. This asymmetry is particularly pronounced in the cross-polarized scattering [Fig. 5(c)]. It is explained by the fact that the cross-polarized component of the mean differential reflection coefficient to the lowest (second) order in the surface profile function is proportional to $g(\mathbf{q}_\parallel - \mathbf{k}_\parallel)\ [(\hat{\mathbf{q}}_\parallel \times \hat{\mathbf{k}}_\parallel)_3]^2$, where $\mathbf{q}_\parallel = (\omega/c)\sin\theta_s(\cos\phi_s \sin\phi_s, 0)$.[23] When the power spectrum $g(\mathbf{k}_\parallel)$ is given by Eq. (18), this function is not symmetric with respect to the plane of incidence.

The co-polarized scattering pattern [Fig. 5(b)] is explained in a similar fashion. In this case the contribution to the mean differential reflection coefficient of the lowest order in the surface profile function contains terms proportional to $g(\mathbf{q}_\parallel - \mathbf{k}_\parallel)(\hat{\mathbf{q}}_\parallel - \hat{\mathbf{k}}_\parallel)^m$ with $m = 1, 2$.[23] The maxima of these functions are in the forward scattering direction and, for an anisotropic surface, move away from the plane of incidence toward the minor axis of the anisotropy.

3. A PENETRABLE SURFACE

3.1 Mathematical Formulation

In calculating the electromagnetic field scattered from a two-dimensional randomly rough surface a convenient starting point are the Franz formulas of electromagnetic scattering theory.[24,25] These formulas for the magnetic and electric fields in the vacuum region $x_3 > \zeta(\mathbf{x}_\parallel)$ can be written as

$$\begin{aligned}\mathbf{H}^{>}(\mathbf{x}|\omega) &= \mathbf{H}(\mathbf{x}|\omega)_{\rm inc} + \frac{1}{4\pi}\boldsymbol{\nabla}\times\int \mathrm{d}^2x'_\parallel\; g_0(\mathbf{x}|\mathbf{x}')|_{x'_3=\zeta(\mathbf{x}'_\parallel)}\mathbf{J}_H(\mathbf{x}'_\parallel|\omega)\\ &\quad -\frac{\mathrm{i}c}{4\pi\omega}\boldsymbol{\nabla}\times\boldsymbol{\nabla}\times\int \mathrm{d}^2x'_\parallel\; g_0(\mathbf{x}|\mathbf{x}')|_{x'_3=\zeta(\mathbf{x}'_\parallel)}\mathbf{J}_E(\mathbf{x}'_\parallel|\omega) \qquad (19a)\end{aligned}$$

$$\begin{aligned}\mathbf{E}^{>}(\mathbf{x}|\omega) &= \mathbf{E}(\mathbf{x}|\omega)_{\rm inc} + \frac{1}{4\pi}\boldsymbol{\nabla}\times\int \mathrm{d}^2x'_\parallel\; g_0(\mathbf{x}|\mathbf{x}')|_{x'_3=\zeta(\mathbf{x}'_\parallel)}\mathbf{J}_E(\mathbf{x}'_\parallel|\omega)\\ &\quad +\frac{\mathrm{i}c}{4\pi\omega}\boldsymbol{\nabla}\times\boldsymbol{\nabla}\times\int \mathrm{d}^2x'_\parallel\; g_0(\mathbf{x}|\mathbf{x}')|_{x'_3=\zeta(\mathbf{x}'_\parallel)}\mathbf{J}_H(\mathbf{x}'_\parallel|\omega). \qquad (19b)\end{aligned}$$

The Franz formulas for the magnetic and electric fields in the scattering medium $x_3 < \zeta(\mathbf{x}_\parallel)$ can be written as

$$\begin{aligned}\mathbf{H}^{<}(\mathbf{x}|\omega) &= -\frac{1}{4\pi}\boldsymbol{\nabla}\times\int \mathrm{d}^2x'_\parallel\; g_\varepsilon(\mathbf{x}|\mathbf{x}')|_{x'_3=\zeta(\mathbf{x}'_\parallel)}\mathbf{J}_H(\mathbf{x}'_\parallel|\omega)\\ &\quad +\frac{\mathrm{i}c}{4\pi\omega}\boldsymbol{\nabla}\times\boldsymbol{\nabla}\times\int \mathrm{d}^2x'_\parallel\; g_\varepsilon(\mathbf{x}|\mathbf{x}')|_{x'_3=\zeta(\mathbf{x}'_\parallel)}\mathbf{J}_E(\mathbf{x}'_\parallel|\omega) \qquad (20a)\end{aligned}$$

$$\begin{aligned}\mathbf{E}^{<}(\mathbf{x}|\omega) &= -\frac{1}{4\pi}\boldsymbol{\nabla}\times\int \mathrm{d}^2x'_\parallel\; g_\varepsilon(\mathbf{x}|\mathbf{x}')|_{x'_3=\zeta(\mathbf{x}'_\parallel)}\mathbf{J}_E(\mathbf{x}'_\parallel|\omega)\\ &\quad -\frac{\mathrm{i}c}{4\pi\omega\varepsilon(\omega)}\boldsymbol{\nabla}\times\boldsymbol{\nabla}\times\int \mathrm{d}^2x_\parallel\; g_\varepsilon(\mathbf{x}|\mathbf{x}')|_{x'_3=\zeta(\mathbf{x}'_\parallel)}\mathbf{J}_H(\mathbf{x}'_\parallel|\omega). \qquad (20b)\end{aligned}$$

In writing these equations we have introduced the vectors

$$\begin{aligned}\mathbf{J}_H(\mathbf{x}_\parallel|\omega) &= \left[\mathbf{n}\times\mathbf{H}^{>}(\mathbf{x}|\omega)\right]\big|_{x_3=\zeta(\mathbf{x}_\parallel)}, \qquad (21a)\\ &= \left[\mathbf{n}\times\mathbf{H}^{<}(\mathbf{x}|\omega)\right]\big|_{x_3=\zeta(\mathbf{x}_\parallel)}, \qquad (21b)\end{aligned}$$

and

$$\begin{aligned}\mathbf{J}_E(\mathbf{x}_\parallel|\omega) &= \left[\mathbf{n}\times\mathbf{E}^{>}(\mathbf{x}|\omega)\right]\big|_{x_3=\zeta(\mathbf{x}_\parallel)}, \qquad (22a)\\ &= \left[\mathbf{n}\times\mathbf{E}^{<}(\mathbf{x}|\omega)\right]\big|_{x_3=\zeta(\mathbf{x}_\parallel)}. \qquad (22b)\end{aligned}$$

The vector $\mathbf{n}$ has been defined in Section 2.1. The scalar free-space Green's function for an infinite scattering medium is defined by

$$\begin{aligned}g_\varepsilon(\mathbf{x}|\mathbf{x}') &= \frac{\exp\left[-\left|\mathbf{x}-\mathbf{x}'\right|/d(\omega)\right]}{\left|\mathbf{x}-\mathbf{x}'\right|} \qquad (23a)\\ &= \int\frac{\mathrm{d}^2k_\parallel}{(2\pi)^2}\,\frac{2\pi}{\beta(k_\parallel)}\exp\left[\mathrm{i}\mathbf{k}_\parallel\cdot(\mathbf{x}_\parallel-\mathbf{x}'_\parallel)\right]\exp\left[-\beta(k_\parallel)|x_3-x'_3|\right], \qquad (23b)\end{aligned}$$

where

$$\beta(k_\parallel) = \left[k_\parallel^2+\frac{1}{d^2(\omega)}\right]^{\frac{1}{2}}, \qquad \mathrm{Re}\,\beta(k_\parallel)>0, \mathrm{Im}\,\beta(k_\parallel)<0, \qquad (24)$$

and $d(\omega) = (c/\omega)[-\varepsilon(\omega)]^{-\frac{1}{2}}$, $\mathrm{Re}\, d(\omega) > 0$, $\mathrm{Im}\, d(\omega) > 0$, while $\varepsilon(\omega)$ is the dielectric function of the scattering medium.

To obtain the equations satisfied by $\mathbf{J}_H(\mathbf{x}_\parallel|\omega)$ and $\mathbf{J}_E(\mathbf{x}_\parallel|\omega)$ we proceed as follows. We take the vector cross product of Eqs. (19a) and (20a) with the vector $\mathbf{n}$, evaluate each product at $x_3 = \zeta(\mathbf{x}_\parallel) + \eta$, and $x_3 = \zeta(\mathbf{x}_\parallel) - \eta$, respectively, where η is a positive infinitesimal, and add the resulting equations. In this way we obtain the equation

$$\begin{aligned}\mathbf{J}_H(\mathbf{x}_\parallel|\omega) &= \mathbf{J}_H(\mathbf{x}_\parallel|\omega)_{\mathrm{inc}} + \frac{1}{4\pi} P \int \mathrm{d}^2 x'_\parallel \, \left[\!\!\left[\mathbf{n} \times \{\boldsymbol{\nabla} \times [g_0(\mathbf{x}|\mathbf{x}') - g_\varepsilon(\mathbf{x}|\mathbf{x}')] \mathbf{J}_H(\mathbf{x}'_\parallel|\omega)\} \right]\!\!\right] \\ &\quad - \frac{\mathrm{i}c}{4\pi\omega} \int \mathrm{d}^2 x'_\parallel \, \left[\!\!\left[\mathbf{n} \times \{\boldsymbol{\nabla} \times \boldsymbol{\nabla} \times [g_0(\mathbf{x}|\mathbf{x}') - g_\varepsilon(\mathbf{x}|\mathbf{x}')] \mathbf{J}_E(\mathbf{x}'_\parallel|\omega)\} \right]\!\!\right], \end{aligned} \tag{25a}$$

where $\mathbf{J}_H(\mathbf{x}_\parallel|\omega)_{\mathrm{inc}} = \mathbf{n} \times \mathbf{H}(\mathbf{x}|\omega)_{\mathrm{inc}}|_{x_3 = \zeta(\mathbf{x}_\parallel)}$, and P denotes the Cauchy principal value.

If we next take the vector cross product of Eq. (19b) and of $\varepsilon(\omega)$ times Eq. (20b) with the vector $\mathbf{n}$, evaluate each product at $x_3 = \zeta(\mathbf{x}_\parallel) + \eta$, and at $x_3 = \zeta(\mathbf{x}_\parallel) - \eta$, respectively, and add the resulting equations, we obtain

$$\begin{aligned}\mathbf{J}_E(\mathbf{x}_\parallel|\omega) &= 2\frac{\mathbf{J}_E(\mathbf{x}_\parallel|\omega)_{\mathrm{inc}}}{1+\varepsilon(\omega)} + \frac{2}{4\pi[1+\varepsilon(\omega)]} P \int \mathrm{d}^2 x'_\parallel \, \left[\!\!\left[\mathbf{n} \times \{\boldsymbol{\nabla} \times [g_0(\mathbf{x}|\mathbf{x}') - \varepsilon(\omega) g_\varepsilon(\mathbf{x}|\mathbf{x}')] \mathbf{J}_E(\mathbf{x}'_\parallel|\omega)\} \right]\!\!\right] \\ &\quad + \frac{2\mathrm{i}c}{4\pi\omega[1+\varepsilon(\omega)]} \int \mathrm{d}^2 x'_\parallel \, \left[\!\!\left[\mathbf{n} \times \{\boldsymbol{\nabla} \times \boldsymbol{\nabla} \times [g_0(\mathbf{x}|\mathbf{x}') - g_\varepsilon(\mathbf{x}|\mathbf{x}')] \mathbf{J}_H(\mathbf{x}'_\parallel|\omega)\} \right]\!\!\right], \end{aligned} \tag{25b}$$

where $\mathbf{J}_E(\mathbf{x}_\parallel|\omega)_{\mathrm{inc}} = \mathbf{n} \times \mathbf{E}(\mathbf{x}|\omega)_{\mathrm{inc}}|_{x_3 = \zeta(\mathbf{x}_\parallel)}$.

In obtaining Eq. (25) we have used the results

$$\begin{aligned}&\lim_{\eta \to 0^+} \int \mathrm{d}^2 x'_\parallel \, \mathbf{n}(\mathbf{x}_\parallel) \times \left\{ \boldsymbol{\nabla} \times \left[g(\mathbf{x}|\mathbf{x}') \Big|_{\substack{x_3 = \zeta(\mathbf{x}_\parallel) \\ x'_3 = \zeta(\mathbf{x}'_\parallel) \pm \eta}} \mathbf{J}(\mathbf{x}'_\parallel|\omega) \right] \right\} \\ &\qquad = \pm 2\pi \, \mathbf{J}(\mathbf{x}_\parallel|\omega) + P \int \mathrm{d}^2 x'_\parallel \, \mathbf{n}(\mathbf{x}_\parallel) \times \left\{ \left[\!\!\left[\boldsymbol{\nabla} \times [g(\mathbf{x}|\mathbf{x}')] \right]\!\!\right] \mathbf{J}(\mathbf{x}'_\parallel|\omega)] \right\}, \end{aligned} \tag{26}$$

where $g(\mathbf{x}|\mathbf{x}')$ is either $g_0(\mathbf{x}|\mathbf{x}')$ or $g_\varepsilon(\mathbf{x}|\mathbf{x}')$, $\mathbf{J}(\mathbf{x}_\parallel|\omega)$ is either $\mathbf{J}_H(\mathbf{x}_\parallel|\omega)$ or $\mathbf{J}_E(\mathbf{x}_\parallel|\omega)$, and P denotes the Cauchy principal value. Equations of the type of Eq. (25) are called Müller integral equations.[26,27] These equations are convenient for numerical calculations. Because $g_0(\mathbf{x}|\mathbf{x}')$ and $g_\varepsilon(\mathbf{x}|\mathbf{x}')$ have the same limiting behavior as $\mathbf{x}' \to \mathbf{x}$, the most divergent terms in the integrands, associated with the second derivatives of these Green's functions, cancel, rendering the resulting integrals integrable. The terms containing the first derivatives of the Green's functions possess integrable singularities.

From the definitions of $\mathbf{J}_{H,E}(\mathbf{x}_\parallel|\omega)$ it follows that $\mathbf{n} \cdot \mathbf{J}_{H,E}(\mathbf{x}_\parallel|\omega) = 0$. Therefore $\mathbf{J}_{H,E}(\mathbf{x}_\parallel|\omega)$ have only two independent elements, which we choose to be $J_{H,E}(\mathbf{x}_\parallel|\omega)_1$ and $J_{H,E}(\mathbf{x}_\parallel|\omega)_2$. The elements $J_{H,E}(\mathbf{x}_\parallel|\omega)_3$ are then obtained from the analogues of Eq. (6). Equations (25) thus provide a system of four coupled, inhomogeneous two-dimensional integral equations for $J_{H,E}(\mathbf{x}_\parallel|\omega)_{1,2}$.

By the use of a local impedance boundary condition,[28]

$$J_E(\mathbf{x}_\parallel|\omega)_i = K_{ij}(\mathbf{x}_\parallel|\omega) J_H(\mathbf{x}_\parallel|\omega)_j \qquad (i = 1, 2), \tag{27}$$

the dependence on $J_E(\mathbf{x}_\parallel|\omega)_{1,2}$ can be removed from Eq. (25a), yielding a pair of coupled, inhomogeneous, two-dimensional, integral equations for $J_H(\mathbf{x}_\parallel|\omega)_{1,2}$. These equations are converted into matrix equations in the manner described in Section 2, which are then solved by the biconjugate gradient stabilized method. The solutions are used to calculate the contribution to the mean differential reflection coefficient from the light scattered incoherently, by the use of the expressions obtained in Section 2.

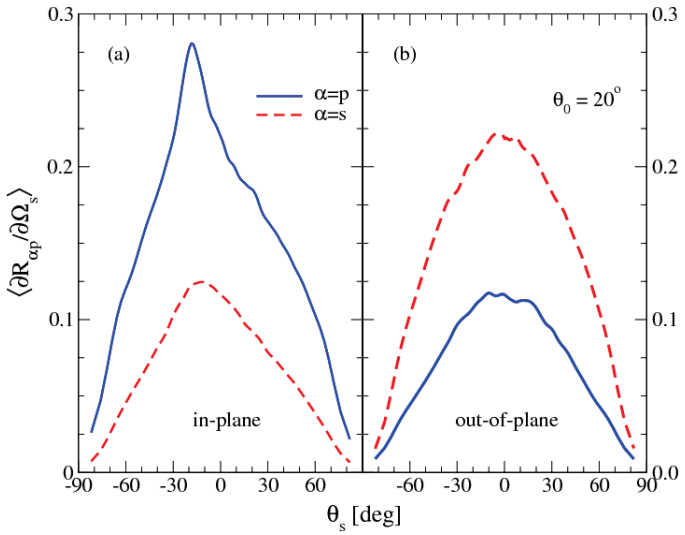

Figure 6. The mean differential reflection coefficients, $\langle \partial R_{\alpha p}/\partial \Omega_s \rangle$ $(p \to \alpha)$ for a p-polarized incident beam of wavelength $\lambda = 632.8$nm and width $w = 4\lambda$, whose polar angle of incidence is $\theta_0 = 20^\circ$, as functions of the polar scattering angle θ_s for the (a) in-plane and (b) out-of-plane scattering. Negative values for θ_s are interpreted as in the caption to Fig. 2. The scattering system assumed in obtaining these results consisted of a silver substrate ($\varepsilon(\omega) = -16 + \mathrm{i}1.088$) separated from vacuum by a Gaussian-correlated randomly rough surface of rms-height $\delta = \lambda/4$ and correlation length $a = \lambda/2$. The randomly rough surface covered an area of $16\lambda \times 16\lambda$ and the discretization length used in the numerical calculations was $\Delta x = \lambda/7$ thus resulting in a 112×112 grid of $\mathbf{x}_\parallel$ values. A total of 5 000 surface realizations were used to calculate $\langle \partial R_{\alpha p}/\partial \Omega_s \rangle$. (After Ref. 14).

3.2 Results for a Penetrable Surface

3.2.1 A Metallic Surface

We first present results for scattering from a metallic surface. We have carried out numerical simulations for the scattering of a p-polarized beam of light of wavelength $\lambda = 632.8$ nm and width parameter $w = 4\lambda$, incident on a randomly rough silver surface. The dielectric function of silver at this wavelength is $\varepsilon(\omega) = -16.00 + \mathrm{i}1.088$.[29] The surface roughness is characterized by the Gaussian power spectrum (16) with a correlation length $a = \lambda/2$, and an rms height $\delta = \lambda/4$. The rough surface was assumed to cover an area $16\lambda \times 16\lambda$ on the mean scattering surface, and the discretization length Δx was $\lambda/7$ on a 112×112 grid of $\mathbf{x}_\parallel$ values.

In Fig. 6 we present the mean differential reflection coefficients as functions of the polar scattering angle θ_s for the in-plane [Fig. 6(a)] and out-of-plane ($\phi_s = \pm 90^\circ$) [Fig. 6(b)], co-(p→p) and cross-(p→s) scattering of the beam when the polar and azimuthal angles of incidence (θ_0, ϕ_0) are $(20^\circ, 0^\circ)$. The results obtained from $N_p = 5\,000$ realizations of the surface profile function were averaged to obtain these results. The calculations required 96 CPU seconds on a 2.67 GHz Intel i7 CPU for each realization of the surface profile function. The peak at $\theta_s = -20^\circ$ in the mean differential reflection coefficient for in-plane co-polarized scattering plotted in Fig. 6(a) is the enhanced backscattering peak.

For the same parameters we present in Figs. 7(a)–(c) the full angular distribution of the mean differential reflection coefficient when the polarization state of the scattered light is not recorded [Fig. 7(a)], when only the p-polarized component of the scattered light is recorded [Fig. 7(b)], and when only the s-polarized component of the scattered light is recorded [Fig. 7(c)]. Similar results, but for an s-polarized incident beam, are presented in Figs. 7(d)–(f). The peaks observed in Figs. 7(a), 7(b), 7(d), and 7(f) in the retroreflection direction ($\theta_s = \theta_0, \phi_s = \phi_0 + 180^\circ$) are the enhanced backscattering peaks.

From a knowledge of the full angular distribution of the mean differential reflection coefficient, the conservation of energy in the scattering process can be checked by means of Eq. (17). For this purpose the full angular distribution of the mean differential reflection coefficient was calculated for "nonabsorbing" silver, *i.e.* for the

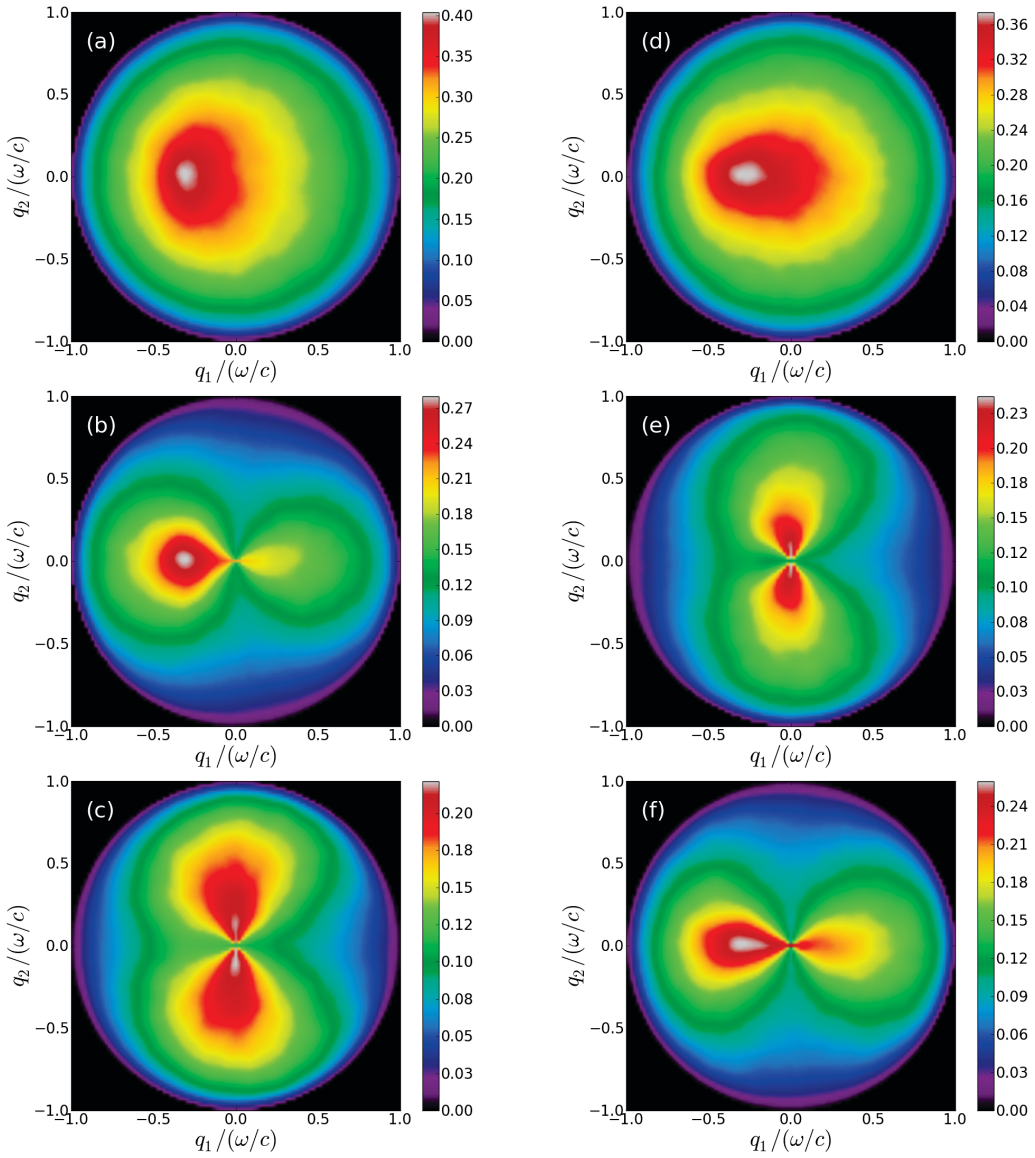

Figure 7. Similar to Fig. 3, but now the scattering medium is silver, and therefore penetrable. The roughness and numerical parameters assumed in obtaining these results are identical to those used to obtain the results of Fig. 6.

case in which the imaginary part of its dielectric function was set equal to zero, so that $\varepsilon(\omega) = -16.00$. For the parameters used in obtaining the results presented in Figs. 6 and 7 it was found that $U_{p,s}(20^\circ, 0^\circ) > 0.995$, a result that demonstrates the accuracy of our computational approach.

In order to obtain such a good unitarity value it was necessary to treat not only the diagonal elements of the matrix versions of Eq. (25) accurately, but also close-to-diagonal elements, because of the singular behavior of the Green's functions for small arguments. The need to treat close-to-diagonal matrix elements more accurately than matrix elements between more widely separated points in the solution of the volume integral equation arising in scattering from finite-sized objects has also been noted.[30] If the extended midpoint method was used in calculating the off-diagonal matrix elements, while the diagonal elements were treated exactly, as in [6] and [9], a value of $U_p(20^\circ, 0^\circ) = 0.834$ was obtained. The ability to calculate unitarity values, and the need to treat close-to-diagonal matrix elements accurately to obtain good unitarity values, are some of the main results of this work.

4. SOLUTION OF THE REDUCED RAYLEIGH EQUATIONS

4.1 Mathematical Formulation

The calculation of the electromagnetic field scattered from a randomly rough surface of a penetrable medium is greatly simplified if the field in the scattering medium does not need to be taken into account. The use of an impedance boundary condition at the interface between the medium of incidence and the scattering medium accomplishes this, so that only the field in the medium of incidence needs to be determined.

The same result can also be achieved by the use of the reduced Rayleigh equation for calculating the scattered field. In this section we present this equation and describe its numerical solution.

We begin by writing the electric field in the vacuum region $x_3 > \zeta(\mathbf{x}_\parallel)$ as the sum of an incident and a scattered field, $\mathbf{E}(\mathbf{x};t) = \left[\mathbf{E}^{(i)}(\mathbf{x}|\omega) + \mathbf{E}^{(s)}(\mathbf{x}|\omega)\right]\exp(-\mathrm{i}\omega t)$, where

$$\mathbf{E}^{(i)}(\mathbf{x}|\omega) = \left\{\frac{c}{\omega}\left[\alpha_0(k_\parallel)\hat{\mathbf{k}}_\parallel + k_\parallel\hat{\mathbf{x}}_3\right]\mathcal{E}_p^{(i)}(\mathbf{k}_\parallel) + [\hat{\mathbf{k}}_\parallel\times\hat{\mathbf{x}}_3]\,\mathcal{E}_s^{(i)}(\mathbf{k}_\parallel)\right\}\exp\left[\mathrm{i}\mathbf{k}_\parallel\cdot\mathbf{x}_\parallel - \mathrm{i}\alpha_0(k_\parallel)x_3\right], \tag{28a}$$

$$\mathbf{E}^{(s)}(\mathbf{x}|\omega) = \int\frac{\mathrm{d}^2q_\parallel}{(2\pi)^2}\left\{\frac{c}{\omega}\left[-\alpha_0(q_\parallel)\hat{\mathbf{q}}_\parallel + q_\parallel\hat{\mathbf{x}}_3\right]\mathcal{E}_p^{(s)}(\mathbf{q}_\parallel) + [\hat{\mathbf{q}}_\parallel\times\hat{\mathbf{x}}_3]\,\mathcal{E}_s^{(s)}(\mathbf{q}_\parallel)\right\}\exp\left[\mathrm{i}\mathbf{q}_\parallel\cdot\mathbf{x}_\parallel + \mathrm{i}\alpha_0(q_\parallel)x_3\right]. \tag{28b}$$

Note that the factors appearing in Eq. (28) in front of $\mathcal{E}_\alpha^{(i)}(\mathbf{k}_\parallel)$ and $\mathcal{E}_\alpha^{(s)}(\mathbf{q}_\parallel)$ ($\alpha = p, s$) are the polarization vectors as defined previously in Section 2.1, but now written out explicitly. Maxwell's equations imply a linear relation between the amplitudes $\mathcal{E}_\alpha^{(s)}(\mathbf{q}_\parallel)$ and $\mathcal{E}_\beta^{(i)}(\mathbf{k}_\parallel)$ of the form ($\alpha = p, s$, $\beta = p, s$)

$$\mathcal{E}_\alpha^{(s)}(\mathbf{q}_\parallel) \;=\; \sum_\beta R_{\alpha\beta}(\mathbf{q}_\parallel|\mathbf{k}_\parallel)\mathcal{E}_\beta^{(i)}(\mathbf{k}_\parallel). \tag{29}$$

The contribution to the mean differential reflection coefficient from the incoherent (diffuse) component of the scattered light, when incident light of β polarization (whose wave vector has the projection $\mathbf{k}_\parallel$ on the mean scattering surface) into light of α polarization (whose wave vector has the projection $\mathbf{q}_\parallel$ on the mean scattering surface), is given by

$$\left\langle\frac{\partial R_{\alpha\beta}}{\partial\Omega_s}\right\rangle_{\mathrm{incoh}} \;=\; \frac{1}{S}\left(\frac{\omega}{2\pi c}\right)^2\frac{\cos^2\theta_s}{\cos\theta_0}\left[\left\langle\left|R_{\alpha\beta}(\mathbf{q}_\parallel|\mathbf{k}_\parallel)\right|^2\right\rangle - \left|\left\langle R_{\alpha\beta}(\mathbf{q}_\parallel|\mathbf{k}_\parallel)\right\rangle\right|^2\right], \tag{30}$$

where S is the area of the plane $x_3 = 0$ covered by the rough surface.

It was shown by Celli and his colleagues[32] by the use of the Rayleigh hypothesis,[33] the extinction theorem,[34] and the vectorial equivalent of the Kirchhoff integral,[35] that the scattering amplitudes $R_{\alpha\beta}(\mathbf{q}_\parallel|\mathbf{k}_\parallel)$ satisfy the matrix integral equation

$$\int\frac{\mathrm{d}^2q_\parallel}{(2\pi)^2}\,\frac{I(\alpha(p_\parallel)-\alpha_0(q_\parallel)|\mathbf{p}_\parallel-\mathbf{q}_\parallel)}{\alpha(p_\parallel)-\alpha_0(q_\parallel)}\,\mathbf{M}(\mathbf{p}_\parallel|\mathbf{q}_\parallel)\mathbf{R}(\mathbf{q}_\parallel|\mathbf{k}_\parallel) = -\frac{I(\alpha(p_\parallel)+\alpha_0(k_\parallel)|\mathbf{p}_\parallel-\mathbf{k}_\parallel)}{\alpha(p_\parallel)+\alpha_0(k_\parallel)}\mathbf{N}(\mathbf{p}_\parallel|\mathbf{k}_\parallel), \tag{31}$$

with R_{pp} and R_{ps} forming the first row of the matrix $\mathbf{R}$, where

$$I(\gamma|\mathbf{Q}_\parallel) \;=\; \int\mathrm{d}^2x_\parallel\exp\left[-\mathrm{i}\gamma\zeta(\mathbf{x}_\parallel)\right]\exp\left[-\mathrm{i}\mathbf{Q}_\parallel\cdot\mathbf{x}_\parallel\right], \tag{32}$$

and $\alpha(p_\parallel) = [\varepsilon(\omega)(\omega/c)^2 - p_\parallel^2]^{\frac{1}{2}}$, with $\mathrm{Re}\,\alpha(p_\parallel) > 0$, $\mathrm{Im}\,\alpha(p_\parallel) > 0$. The matrices $\mathbf{M}(\mathbf{p}_\parallel|\mathbf{q}_\parallel)$ and $\mathbf{N}(\mathbf{p}_\parallel|\mathbf{k}_\parallel)$ are given by

$$\mathbf{M}(\mathbf{p}_\parallel|\mathbf{q}_\parallel) \;=\; \begin{pmatrix} [p_\parallel q_\parallel + \alpha(p_\parallel)\hat{\mathbf{p}}_\parallel\cdot\hat{\mathbf{q}}_\parallel\alpha_0(q_\parallel)] & -\frac{\omega}{c}\alpha(p_\parallel)\,[\hat{\mathbf{p}}_\parallel\times\hat{\mathbf{q}}_\parallel]_3 \\ \frac{\omega}{c}[\hat{\mathbf{p}}_\parallel\times\hat{\mathbf{q}}_\parallel]_3\,\alpha_0(q_\parallel) & \frac{\omega^2}{c^2}\hat{\mathbf{p}}_\parallel\cdot\hat{\mathbf{q}}_\parallel \end{pmatrix} \tag{33a}$$

and

$$\mathbf{N}(\mathbf{p}_\parallel|\mathbf{k}_\parallel) \;=\; \begin{pmatrix} [p_\parallel k_\parallel - \alpha(p_\parallel)\hat{\mathbf{p}}_\parallel\cdot\hat{\mathbf{k}}_\parallel\alpha_0(k_\parallel)] & -\frac{\omega}{c}\alpha(p_\parallel)\,[\hat{\mathbf{p}}_\parallel\times\hat{\mathbf{k}}_\parallel]_3 \\ -\frac{\omega}{c}[\hat{\mathbf{p}}_\parallel\times\hat{\mathbf{k}}_\parallel]_3\,\alpha_0(k_\parallel) & \frac{\omega^2}{c^2}\hat{\mathbf{p}}_\parallel\cdot\hat{\mathbf{k}}_\parallel \end{pmatrix}. \tag{33b}$$

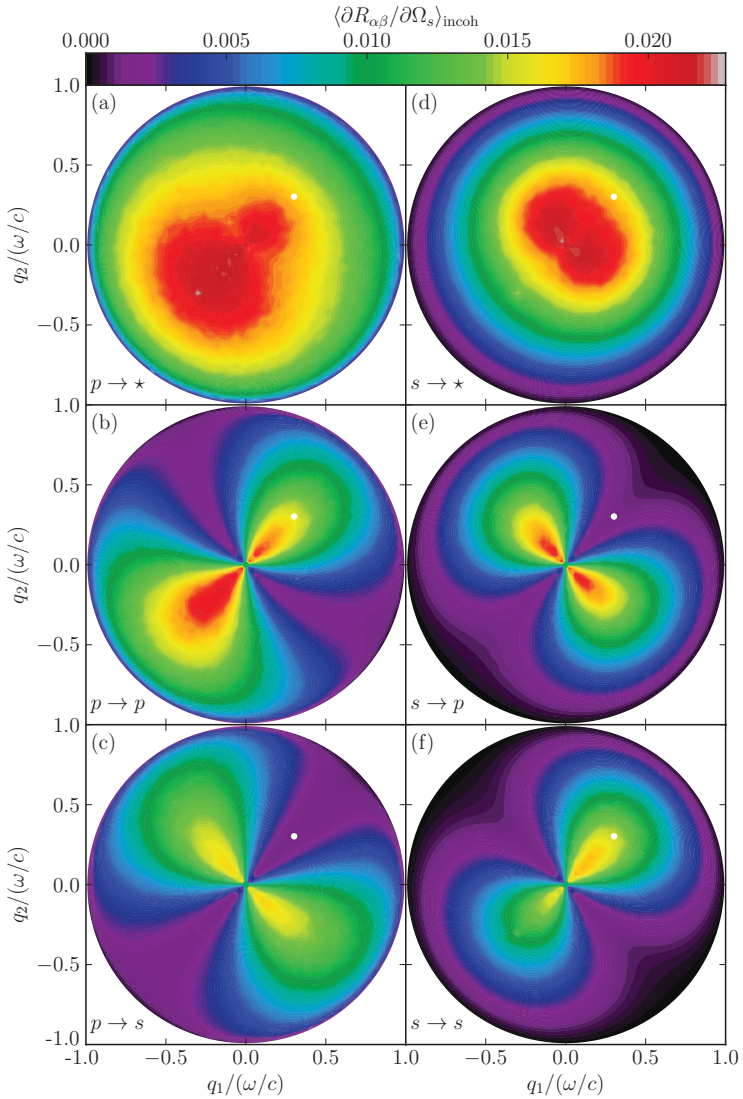

Figure 8. Full angular intensity distribution of the light scattered incoherently from a two-dimensional randomly rough silver surface calculated by solving the reduced Rayleigh equations. Light of either p (left column) or s polarization (right column) is incident on the surface at angles of incidence $(\theta_0, \phi_0) = (25°, 45°)$. The wavelength (in vacuum) of the incident light is $\lambda = 632.8\,\text{nm}$ for which frequency $\omega = 2\pi/\lambda$ the dielectric function of silver is $\varepsilon(\omega) = -16.0 + 1.088\text{i}$. The white dots indicate the position of the specular direction. The surface parameters assumed in these calculations are $L = 25\lambda$; $\delta = \lambda/40$; and $a = \lambda/4$. The surface was discretized so that $Q = 6.4\omega/c$ or equivalently $\Delta x = \pi/Q \approx 0.0781\lambda$. Figures 8(a)–(c) correspond to a p-polarized plane incident wave, while in Figs. 8(d)–(f) the incident plane wave is s polarized. In Figs. 8(a) and (d) all scattered light is recorded, *i.e.* no distinction is made between scattered p- and s-polarized light. However, in Figs. 8(b) and (e) only the scattered p-polarized light is recorded, while Figs. 8(c) and (f) include only s-polarized scattered light. The presented figures were obtained by averaging the results for the differential reflection coefficient obtained for $N_p = 10\,000$ surface realizations.

Although purely numerical, nonperturbative solutions of the reduced Rayleigh equations for the scattering of light from one-dimensional randomly rough clean metal surfaces[36,37] and coated perfectly conducting surfaces[38,39] have been carried out, up to now Eq. (31) has been solved only by small-amplitude perturbation theory through terms of third order in the surface profile fuction.[23,40,41] Here we present some preliminary results for the mean differential reflection coefficient obtained by a purely numerical, nonperturbative solution of Eqs. (31)–(33). This was done by generating a realization of the surface profile as this was done in the preceding two sections, and evaluating the function $I(\gamma|\mathbf{Q}_\parallel)$ by expanding the integrand in Eq. (32) in powers of $\zeta(\mathbf{x}_\parallel)$, and

calculating the Fourier transform of $\zeta^n(\mathbf{x}_\parallel)$ by the Fast Fourier Transform. As in previous sections, the random surface covered a square region of the x_1x_2 plane of edge L, and a grid of N^2 points was created within this square so that the (linear) sampling interval is $\Delta x = L/N$. The infinite limits of integration in Eq. (31) were replaced by finite ones: $|q_1| < Q/2$, $|q_2| < Q/2$ where $Q = \pi/\Delta x$. A quadratic grid within the square region of the q_1q_2 plane of edge Q was constructed with a grid constant $\Delta q = 2\pi/L$. The integral over this region in Eq. (31) was carried out by a two-dimensional version of the extended midpoint method, and the values of $R_{\alpha\beta}(\mathbf{q}_\parallel|\mathbf{k}_\parallel)$ were calculated for values of $\mathbf{q}_\parallel$ at the points of this grid for a given value of $\mathbf{k}_\parallel$, which was a point on the same grid. The resulting matrix equations were solved by LU factorization. This is a slower solution method than the biconjugate gradient stabilized method, but has the advantage of being able to handle multiple right-hand sides, *i.e.* different angles of incidence, more-or-less with no extra addition to the computational time. With the reflection amplitudes, $R_{\alpha\beta}(\mathbf{q}_\parallel|\mathbf{k}_\parallel)$, available, the differential reflection coefficient was then calculated by the use of Eq. (30).

4.2 Results Obtained by the Solution of the Reduced Rayleigh Equations

4.2.1 A Metallic Surface

As the first example of the application of this approach to the scattering of light from a penetrable surface we apply it to the scattering of a p- or s-polarized plane wave of wavelength $\lambda = 632.8$ nm incident on a silver surface. The dielectric function of silver at this wavelength is $\varepsilon(\omega) = -16 + \mathrm{i}1.088$.[29] The roughness of the surface was characterized by the Gaussian power spectrum, Eq. (16), where the transverse correlation length was given the value $a = \lambda/4$, while the rms height of the surface was $\delta = \lambda/40$. In the calculations the rough surface was assumed to cover an area of $25\lambda \times 25\lambda$ of the plane $x_3 = 0$, while for the wavenumber cut-off we assumed $Q = 6.4\omega/c$, which corresponds to a spatial discretization interval of $\Delta x = \pi/Q \approx 0.0781\lambda$ (for both directions).

In Fig. 8 we present contributions to the mean differential reflection coefficients from the light scattered incoherently as functions of q_1 and q_2 when a plane wave is incident on the surface at angles $(\theta_0, \phi_0) = (25°, 45°)$. Figure 8(a) corresponds to a p-polarized incident plane wave being scattered by the rough surface into both p- and s-polarized light, *i.e.* the polarization state of the scattered light was not recorded. However, in Figs. 8(b) and 8(c) contour plots of the same quantity are presented for the cases where only p-polarized or s-polarized scattered light, respectively, are recorded. Similar results are presented in Figs. 8(d)–(f) for the case when the incident light is s-polarized. An arithmetic average of results obtained for $N_p = 10\,000$ realizations of the surface profile function was carried out to produce Fig. 8.

By artificially putting the imaginary part of the dielectric constant of the metal to zero, $\mathrm{Im}\,\varepsilon(\omega) \equiv 0$, so that there is no absorption in the scattering system, it has been found that the numerical method used to solve the reduced Rayleigh equation, Eq. (31), conserves energy with an error smaller than 0.5% for the parameters assumed here.

The numerical calculations used to obtain the results of Fig. 8 required for each realization of the surface profile function approximately 8.8 cpu hours on a single 12-core 2.4 GHz AMD Opteron computer node and using approximately 20 GB of memory.

The calculations whose results are presented in Fig. 8 and which were performed by solving numerically the reduced Rayleigh equations (31), could also have been done by solving the Müller equations, as was discussed in Section 3. In order to compare the two approaches, we present in Fig. 9 the results obtained by these two methods for the contributions to the mean differential reflection coefficients from the light scattered incoherently as functions of the polar scattering angle θ_s for the in-plane ($\phi_s = 0°, 180°$) and out-of-plane ($\phi_s = \pm 90°$) co-($s \to s$) and cross-($s \to p$) polarized scattering when an s-polarized wave is incident on the surface at angles of incidence $(\theta_0, \phi_0) = (25°, 0°)$. The roughness parameters assumed in obtaining these results are identical to those assumed in obtaining Fig. 8. The numerical parameters used to obtain these results were those of Fig. 8 when using the reduced Rayleigh equation. However, when solving the Müller equations, a Gaussian beam of width ($w = 4\lambda$) was assumed to be incident on the surface, which was discretized with an interval $\Delta x = \lambda/7$ (in both directions). It is observed from Fig. 9 that the two approaches produce quantitatively similar results. The minor differences between the results of the two approaches we believe are due to the differences in the areas covered by the rough surfaces, and to the differences in the discretization intervals, assumed in the two sets of calculations, which have not been optimized as yet.

From the results presented in Figs. 8 and 9, we can draw the conclusions that a purely numerical, nonperturbative solution of the reduced Rayleigh equation yields accurate results for the mean differential reflection coefficient that are in good agreement with those obtained by the use of the Müller equations.

4.2.2 A Dielectric Surface

The reduced Rayleigh equation (31) can also be used for calculating the field scattered from a dielectric surface. We apply it here to calculate the contribution to the mean differential reflection coefficient from the incoherent component of the scattered light when a p- or s-polarized plane wave whose wavelength in vacuum is $\lambda = 632.8$ nm is incident at $(\theta_0, \phi_0) = (27.5°, 45°)$ on the surface of a dielectric medium whose dielectric constant is assumed to be $\varepsilon_d = 2.64$ (photoresist). The results are presented in Fig. 10. The randomly rough surface had an rms roughness of $\delta = 3\lambda/200 = 0.015\lambda$ and it covered a $20\lambda \times 20\lambda$ area in the $x_3 = 0$ plane. Moreover, the wavenumber cut-off assumed in these calculations was $Q = 8\omega/c$, corresponding to a discretization interval of $\Delta x = \pi/Q = 0.0625\lambda$. Except for these differences, the remaining roughness and computational parameters were the same as the ones assumed in the calculations that produced Fig 8.

By comparing Figs. 8 and 10 it is observed that the overall structure of the angular distributions of the intensity of the light scattered from a metal and dielectric is rather similar, and that, as expected, the scattered intensity for the metallic surface is stronger (by a factor of about 70) than that for the dielectric surface.

5. DISCUSSION AND CONCLUSIONS

We have shown that the use of the method of moments and the biconjugate gradient stabilized method provides a formally exact solution to the scattering of p- and s-polarized light from a two-dimensional randomly rough perfectly conducting surface, with a modest expenditure of computational time. The addition of an impedance boundary condition on a two-dimensional rough surface to these two methods has been shown to provide a formally exact solution to the scattering of polarized light from two-dimensional randomly rough metallic surfaces, also with a modest expenditure of computational time.

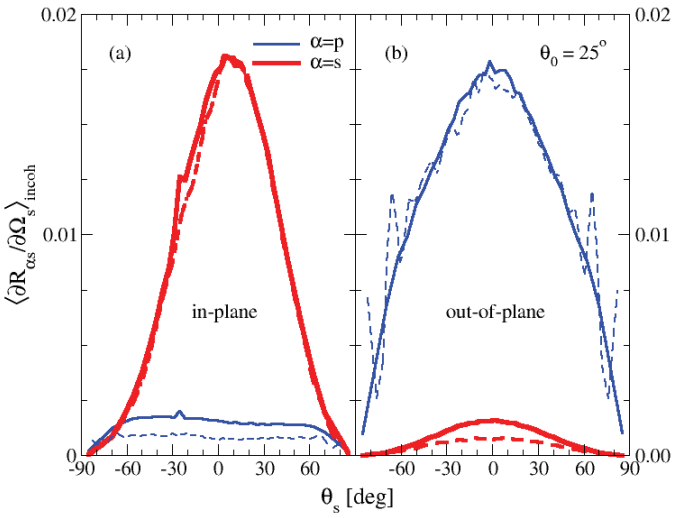

Figure 9. Comparison of the mean differential reflection coefficients for the scattering of s polarized waves from a rough silver surface with the roughness parameters given in the caption of Fig. 8. The results were obtained by two different numerical approaches: the solution of the reduced Rayleigh equation (solid lines), and by the use of the rigorous approach (dashed lines). The numerical parameters and number of surface realizations assumed when using the former approach were those used to obtain the results presented in Fig. 8. However, when using the rigorous approach, the parameters given in the caption to Fig. 6 were assumed with the exception that now $\theta_0 = 25°$, $L = 20\lambda$, and only a small number of surface realizations were used ($N_p = 750$) to obtain these results.

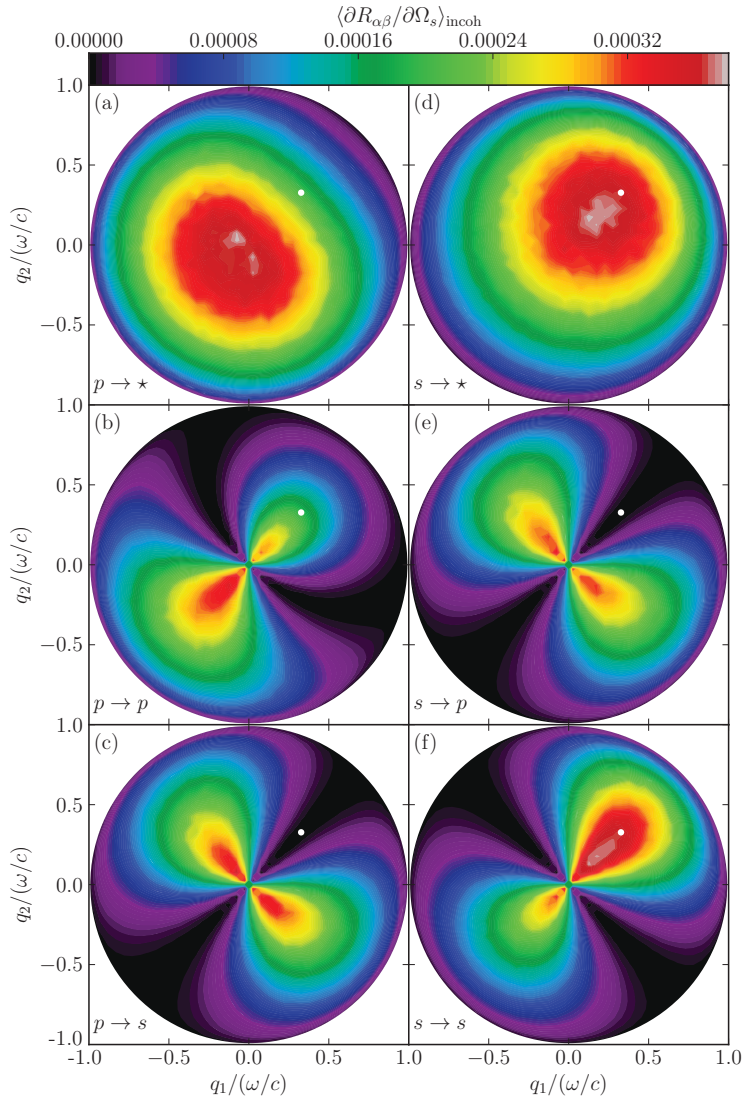

Figure 10. Full angular intensity distribution of the light scattered incoherently from a two-dimensional randomly rough dielectric surface calculated by solving the reduced Rayleigh equations. The dielectric substrate was taken to be photoresist which at the frequency of the incident light $\lambda = 632.8\,\text{nm}$ is characterized by a dielectric constant $\varepsilon(\omega) = 2.64$. The angles of incidence assumed are $(\theta_0, \phi_0) = (27.5^\circ, 45^\circ)$, and the white dots indicate the position of the specular direction. These figures were obtained by averaging results for the scattered intensity obtained for $N_p = 6\,000$ surface realizations. The surface parameters assumed in these calculations were $L = 20\lambda$; $\delta = 3\lambda/200 = 0.015\lambda$; and $a = \lambda/4$. The surface discretization was done so that $Q = 8\omega/c$, or equivalently, $\Delta x = \pi/Q = 0.0625\lambda$. The remaining parameters and the organization of the sub-figures are identical to those of Fig. 8.

The computational methods employed in these calculations have made it possible to obtain a formally exact full angular distribution of the intensity of the light scattered from a strongly rough random surface. In the case of scattering from a perfectly conducting surface, and from a metallic surface when the imaginary part of its dielectric function is set equal to zero, knowledge of the full angular distribution of the intensity of the scattered light enables the conservation of energy in the scattering process to be checked. It was found to be satisfied with an error smaller than 0.5%, a result that testifies to the accuracy of the methods used in our calculations and the adequacy of the discretization of the mean scattering surface employed in them.

We have also presented results obtained from a rigorous numerical solution of the reduced Rayleigh equation for the scattering of p- and s-polarized light from a penetrable surface. These results demonstrate the feasibility

of using this equation in studies of the scattering of light from weakly rough surfaces. The good agreement between the results obtained by the solution of the reduced Rayleigh equation and those obtained by the use of the rigorous computational method indicates that the simpler approach yields accurate results for scattering from surfaces that are not very rough. The limits of validity of this equation have yet to be determined.

The success of the methods used in carrying out the calculations described here opens the door to rigorous computational studies of other properties of electromagnetic waves scattered from two-dimensional randomly rough surfaces. These include calculations of the ellipsometric parameters of metallic and dielectric surfaces, transmission through dielectric surfaces, and all of the elements of the Mueller matrix for scattering from and transmission through such surfaces. This work will be reported elsewhere.

ACKNOWLEDGMENTS

The research of T.A.L. and A.A.M. was supported in part by AFRL contract FA9453-08-C-0230. The research of I.S. was supported in part by the Research Council of Norway (Småforsk Grant). We are grateful to NOTUR (the Norwegian Metacenter for Computational Science) for the allocation of computer time.

REFERENCES

1. P. Tran, V. Celli, and A.A. Maradudin, "Electromagnetic scattering from a two-dimensional, randomly rough, perfectly conducting surface: Iterative methods," J. Opt. Soc. Am. A **11**, 1685–1689 (1994).
2. R.L. Wagner, J. Song, and W.C. Chew, "Monte Carlo simulation of electromagnetic scattering from two-dimensional random rough surfaces," IEEE Trans. Antennas Propag. **45**, 235–245 (1997).
3. K. Pak, L. Tsang, C.H. Chan, and J.T. Johnson, "Backscattering enhancement of electromagnetic waves from two-dimensional perfectly conducting random rough surfaces based on Monte Carlo simulations," J. Opt. Soc. Am. A **12**, 2491–2499 (1995).
4. J.T. Johnson, L. Tsang, R.T. Shin, K. Pak, C.H. Chan, A. Ishimaru, and Y. Kuga, "Backscattering enhancement of electromagnetic waves from two-dimensional perfectly conducting random rough surfaces: a comparison of Monte Carlo simulations with experimental data," IEEE Trans. Antennas Propag. **44**, 748–756 (1996).
5. D. Torrungrueng, H.-T. Chou, and J.T. Johnson, "A novel acceleration algorithm for the computation of scattering from two-dimensional large-scale perfectly conducting random rough surfaces with the forward-backward method," IEEE Trans. Geosci. Remote Sensing **38**, 1656–1668 (2000).
6. G. Soriano and M. Saillard, "Scattering of electromagnetic waves from two-dimensional rough surfaces with an impedance approximation," J. Opt. Soc. Am. A **18**, 124–133 (2001).
7. I. Simonsen, A.A. Maradudin, and T.A. Leskova, "Scattering of electromagnetic waves from two-dimensional randomly rough perfectly conducting surfaces: The full angular intensity disribution," Phys. Rev. A **81**, 013806 (1–13) (2010).
8. I. Simonsen, J.B. Kryvi, A.A. Maradudin, and T.A. Leskova, "Light scattering from anisotropic, randomly rough, perfectly conducting surfaces," Comp. Phys. Commun. **182**, 1904–1908 (2011).
9. P. Tran and A.A. Maradudin, "Scattering of electromagnetic waves from a randomly rough 2D metallic surface," Opt. Commun. **110**, 269–273 (1994).
10. L. Tsang, C.H. Chan, and K. Pak, "Backscattering enhancement of a two-dimensional random rough surface (three-dimensional scattering) based on Monte Carlo simulations," J. Opt. Soc. Am. A **11**, 711–715 (1994).
11. K. Pak, L. Tsang, and J.T. Johnson, "Numerical simulations and backscattering enhancement of electromagnetic waves from two-dimensional dielectric random rough surfaces with the sparse-matrix canonical grid method," J. Opt. Soc. Am. A **14**, 1515–1529 (1997).
12. N. Engheta, W.D. Murphy, V. Rokhlin, and M.S. Vassiliou, "The fast multipole method (FMM) for electromagnetic scattering problems," IEEE Trans. Antennas Propag. **40**, 634–641 (1992).
13. V. Jandhyala, B. Shanker, E. Michielssen and W.C. Chew, "Fast algorithm for the analysis of scattering by dielectric rough surfaces," J. Opt. Soc. Am. A **15**, 1877–1885 (1998).
14. I. Simonsen, A.A. Maradudin, and T.A. Leskova, "Scattering of electromagnetic waves from two-dimensional randomly rough penetrable surfaces," Phys. Rev. Lett. **104**, 223904 (1–4) (2010).

15. A.A. Maradudin, T. Michel, A.R. McGurn, and E.R. Méndez, "Enhanced backscattering of light from a random grating," Ann. Phys. (N.Y.) **203**, 255–307 (1990).
16. J.A. Kong, *Electromagnetic Theory*, 3rd ed. (EMW Publishing, Cambridge, MA, 2005), p. 674.
17. W.H. Press, S.A. Teukolsky, W.T. Vetterling, and B. P. Flannery, *Numerical Recipes in Fortran*, 2nd ed. (Cambridge, University Press, New York, 1992), p. 129.
18. H. Van der Vorst, "Bi-CGSTAB: A fast and smoothly converging variant of Bi-CG for the solution of nonsymmetric linear systems," SIAM J. Sci. Stat. Comp. **13**, 631–644 (1992).
19. A.R. McGurn, A.A. Maradudin and V. Celli, "Localization effects in the scattering of light from a randomly rough grating," Phys. Rev. B**31**, 4866–4871 (1985).
20. E.R. Méndez and K.A. O'Donnell, "Observation of depolarization and backscattering enhancement in light scattering from Gaussian random surfaces," Opt. Commun. **61**, 91–95 (1987).
21. D. Torrungrueng and J.T. Johnson, "Numerical studies of backscattering enhancement of electromagnetic waves from two-dimensional random rough surfaces with the forward-backward/novel spectral acceleration method," J. Opt. Soc. Am. A **18**, 2518–2526 (2001).
22. E.I. Chaikina, P. Negrete-Regagnon, V. Ruiz-Cortés, and E.R. Méndez, "Measurements of the hemispherical scattering distribution function of rough dielectric surfaces," Opt. Commun. **205** 215–221 (2002).
23. A.R. McGurn and A.A. Maradudin, "Perturbation theory results for the diffuse scattering of light from two-dimensional randomly rough surfaces," Waves in Random Media **6**, 251–267 (1996).
24. W. Franz, "Zur Formulierung des Huygenschen Prinzips," Z. Naturforsch. **3a**, 500–506 (1948).
25. Ref. 16, pp. 674–675.
26. C. Müller, *Foundations of the Mathematical Theory of Electromagnetic Waves* (Springer-Verlag, Berlin, 1969), Secs. 21 and 23.
27. N. Morita, N. Kumagai, and J.R. Mautz, *Integral Equation Methods for Electromagnetics* (Artech House, Boston, 1990), Sec. 3.5.2.
28. A.A. Maradudin, "The impedance boundary condition at a two-dimensional rough metal surface," Opt. Commun. **116**, 452–467 (1995).
29. P.B. Johnson and R.W. Christy, "Optical Constants of the Noble Metals," Phys. Rev. B **6**, 4370–4379 (1972).
30. J.P. Kotthaus and O.J.F. Martin, "Accurate solution of the volume integral equation for high-permittivity scatterers," IEEE Trans. Antennas Propag. **48**, 1719-1726 (2000).
31. A.A. Maradudin and E.R. Méndez, "The utility of an impedance boundary condition in the scattering of light from one-dimensional randomly rough dielectric surfaces," Opt. Spectrosc. **80**, 409–420 (1996).
32. G.C. Brown, V. Celli, M. Haller, and A. Marvin, "Vector theory of light scattering from a rough surface: unitary and reciprocal expansions," Surf. Sci. **136**, 381–397 (1984).
33. Lord Rayleigh, *The Theory of Sound*, 2nd ed. (Dover, New York, 1945), vol. II, pp. 89-96, pp. 297–311.
34. E. Wolf, "A generalized extinction theorem and its role in scattering theory," in *Coherence and Quantum Optics*, eds. L. Mandel and E. Wolf (Plenum, New York, 1973), pp. 339-357.
35. J.D. Jackson, *Classical Electrodynamics*, 2nd ed. (Wiley, New York, 1962), Section 9.9.
36. T.R. Michel, "Resonant light scattering from weakly rough random surfaces and imperfect gratings," J. Opt. Soc. Am. A **11**, 1874–1885 (1994).
37. T.R. Michel, M.E. Knotts and K.A. O'Donnell, "Scattering by plasmon polaritons on a rough surface with a periodic component," J. Opt. Soc. Am. A **12**, 548–559 (1995).
38. A. Madrazo and A.A. Maradudin, "Numerical solution of the reduced Rayleigh equation for the scattering of electromagnetic waves from a rough dielectric film on perfectly conducting substrates," Opt. Commun. **134**, 251–263 (1997).
39. I. Simonsen and A.A. Maradudin, "Numerical solution of of electromagnetic waves scattered from planar dielectric films deposited on rough perfectly conducting substrates," Opt. Commun. **162**, 99–111 (1999).
40. J.T. Johnson, "Third order small perturbation method for scattering from dielectric rough surfaces," J. Opt. Soc. Am. A **16**, 2720–2736 (1999).
41. A. Soubret, G. Berginc, and C. Bourrely, "Application of reduced Rayleigh equations to electromagnetic wave scattering by two-dimensional randomly rough surfaces," Phys. Rev. B **63**, 245411 (1–20) (2003).